REVIEW

ADVANCED
INTELLIGENT
SYSTEMS
Open Access

www.advintellsyst.com

The Encoding of Light-Driven Micro/Nanorobots: from Single to Swarming Systems

Jizhuang Wang, Ze Xiong,* and Jinyao Tang*

Light-driven micro/nanorobot (LMNR), as an artificial micro/nanomachine, manifests excellent controllability, and appealing applications. The development of light-manipulation strategies significantly advance both single and swarming LMNR systems, improving their capability for sophisticated tasks. In this review, the existing manipulation strategies for LMNRs, which are categorized according to encoding methods of light signals, is summarized. On top of it, the swarming systems are overviewed by considering the field in charge. The emerging applications and major challenges of LMNRs are then presented and discussed, which may lend insight to researchers to develop bespoke LMNR systems for target applications.

1. Introduction

"Robot", since its first introduction by Czech writer Karel Čapek in his play *Rossum's Universal Robots*, has inspired numerous science fiction and academic studies. Beyond the humanoid machine with creative thinking and emotional response, robotic devices that can perform precise and laborious tasks, with/without the aid of human operators, are indispensable in the modern industry and our daily life. With the help of teleoperation techniques, robotic devices can extend the sensation and manipulation capabilities of humans and get access to unsafe or hard-to-reach spaces. Light-driven micro/nanorobot (LMNR), as an emerging semi-autonomous robot, can be remotely controlled by diverse light signals.[1–3] Inspired by the multiplexing techniques (space, frequency, polarization-division, etc.) widely used in telecommunications, the LMNRs can also be manipulated by encoded light signals.

Dr. J. Wang
College of Chemistry and Materials Science
Jinan University
Guangzhou 510632, P. R. China

Dr. Z. Xiong, Prof. J. Tang
Department of Chemistry
The University of Hong Kong
Pokfulam Road, Hong Kong, China
E-mail: zexiong@connect.hku.hk; jinyao@hku.hk

(iD) The ORCID identification number(s) for the author(s) of this article can be found under https://doi.org/10.1002/aisy.202000170.

Its exemption from onboard signal processing and energy storage makes the robotic system at micro/nanoscale possible, promising a variety of unprecedented applications, ranging from noninvasive surgery,[4,5] manufacturing,[6] biosensing,[7] to environmental remediation.[8]

In addition to LMNRs, micro/nanorobots (MNRs) can also be driven and controlled by electric, magnetic or acoustic field, as well as solely by chemical reactions, which have demonstrated dexterous manipulation and appealing applications,[9–11] and been discussed in other excellent reviews over the past decade.[12–16] These MNRs showcased respective pros and cons, depending on the specific target application. Particularly, for the operation in the biological environment, most of the MNRs are facing challenges from biocompatibility, efficiency, and manipulation accuracy,[17] which call for further development in both fundamental mechanisms and system design. Regarding the propulsion mechanism, LMNRs can be driven by electrophoresis,[18–20] diffusiophoresis,[21] thermophoresis,[22,23] bubble propulsion,[24] and deformation propulsion.[25,26] The communication and cooperation between individual LMNRs will elicit novel swarming behaviors and enhance their abilities, which is ubiquitous in nature,[27–29] but still in infancy for robotic systems.[30,31]

Here, we will first revisit the primary modes for light signal encoding in Section 2, which can be briefly categorized into spatial, frequency, and polarization encoding modes. These modes can increase the degrees of freedom for controlling LMNRs, allowing a multiplexed LMNRs system, which is of great importance for performing comprehensive tasks by a large group of LMNRs. To further enhance the controllability and functionality of LMNRs, LMNRs integrated with other encoding signals are introduced in Section 3, highlighting hybrid systems with benefits from respective fields. Section 4 discusses the techniques to assemble multiple LMNRs and the swarming behaviors therein. After that, the urgent challenges concerning the emerging applications of LMNRs, particularly for biomedical applications, are examined and discussed in Section 5, for instance, ion tolerance, propulsion efficiency, and biofouling. Finally, we summarize this review and give an outlook on the future development of LMNRs. Although the synthesis and preparation of LMNRs are also of great importance for the study and application of LMNRs, most of the developments have already been systematically reviewed in recent literature,[32,33] thus will not be covered here.

**ADVANCED
SCIENCE NEWS**

www.advancedsciencenews.com

**ADVANCED
INTELLIGENT
SYSTEMS**
Open Access

www.advintellsyst.com

2. Primary Encoding Modes for LMNRs

Light, or more generally electromagnetic waves, is the foundation of modern communication techniques due to its flexibility of modulation. It can be encoded to offer precise control over LMNRs through three major modes: 1) spatial encoding mode, 2) polarization encoding mode, and 3) frequency encoding mode (**Figure 1**). These diverse encoding modes provided plentiful space for LMNRs design, empowering single and swarming LMNR systems to realize complex manipulation, including but not limited to nanosurgery and micromanufacturing.

2.1. Spatial Encoding Mode for LMNRs

Optical tweezers, as one of the most powerful and well-developed techniques for micro/nano object manipulation, were introduced by Ashkin et al. at AT&T Bell Laboratories in 1986[34] and awarded Nobel Prize in Physics 2018. To realize the micromanipulation with optical tweezers, a tightly focused laser beam forms a spatially distributed intensity gradient, which induces an electric dipole moment and light refraction in small and large objects, respectively, driving the micro/nano object toward the focal point (**Figure 2**a). Optical tweezers have significantly fueled the studies in physics, chemistry, and biology.[14,35] Its capability is developed from single target manipulation to multiple targets manipulation, from transparent dielectric colloid to metal nanoparticles[36,37] and other exotic structures.[38,39] The spatially confined focus point facilitated the manipulation in three-dimensional (3D) space, which also inspired fabrication techniques at micro/nanoscale.[40] However, one limitation of optical tweezer is the small momentum of the photon. To effectively manipulate micro/nanoparticles, a strong light with intensity up to $GW\,cm^{-2}$ range is required,[41] which weakens the

otherwise even greater applications beyond research. Therefore, many alternatives are being developed to realize similar versatility of optical tweezers with much lower light intensity.

Optoelectric tweezers, although shares a similar name of optical tweezers, use electrokinetic and electrohydrodynamic forces created by the electric field to manipulate objects, while a structured light is used to pattern the electric field on the photoconductive electrode. This method can greatly reduce the required light intensity and can control much larger objects in comparison with the traditional optical tweezers (Figure 2b).[42] Due to the low light intensity requirement, the structured light can be easily created by a stationary photomask or a computer-controlled digital light processing (DLP) projector.[43] Such merit greatly facilitated the maneuver of a large population of particles or an entity with a larger size. For instance, the irregularly shaped light field can be implemented, enabling the manipulation of submillimeter optoelectronic SU-8 robot for a series of load, transport, and deliver tasks (Figure 2c).[43] Moreover, the DLP technique can spontaneously support separated light patterns with distinct photon frequencies in one scanning field, which is favorable for the frequency encoding mode, as will be discussed later.

As a nontrivial property of light, the wavefronts of light contained a great amount of information that can be used for computing, manipulation, and imaging.[44,45] Currently, this degree of freedom has yet been extensively explored in the LMNR system, with the exception of the propagation direction of light. Such propagation direction is the simplest information contained in the wavefront of light and ubiquitously influences the motion behaviors of creatures in nature, which is usually referred to as phototaxis.[46] As a counterpart of phototaxis in the artificial system, LMNR also demonstrated positively or negatively phototactic behaviors by shadowing effect and surface charge programming (Figure 2d).[47] Such shadowing effect is induced by nonuniform excitation of LMNR with a configured incident direction of light, which promised navigation of LMNR without additional auxiliary magnetic or acoustic field. Moreover, this phototactic behavior can be realized in LMNRs with much simpler structures (Figure 2e),[48–50] suggesting its universal existence and widespread applications. Most recently, a liquid droplet containing photochromic molecules was proposed as a micromotor, where both positive and negative phototaxis were realized by generating Marangoni flow at the water/oil interface upon unbalanced illumination (Figure 2f).[51] This study enriched the inventory of LMNRs, envisioning applications from microreactor, biosensing to liquid cargo transportation.

2.2. Polarization Encoding Mode for LMNRs

Polarization-division multiplexing is a technique to transmit two channels of information with two orthogonally polarized electromagnetic waves, which has been widely adopted in point-to-point microwave communication. In optical tweezers, the polarized light has been exploited for both linearly[52,53] and circularly[54,55] polarized optical manipulations, while the high light intensity is generally needed. To explore the polarization-based optical manipulation, the materials with strong dichroism is needed to distinguish incident light with different polarizations.
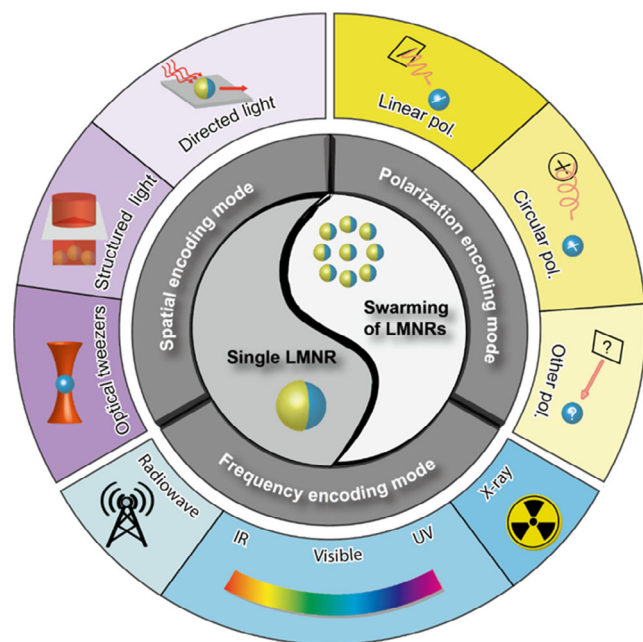

Figure 1. Primary encoding modes and specific strategies for the manipulation of LMNRs.
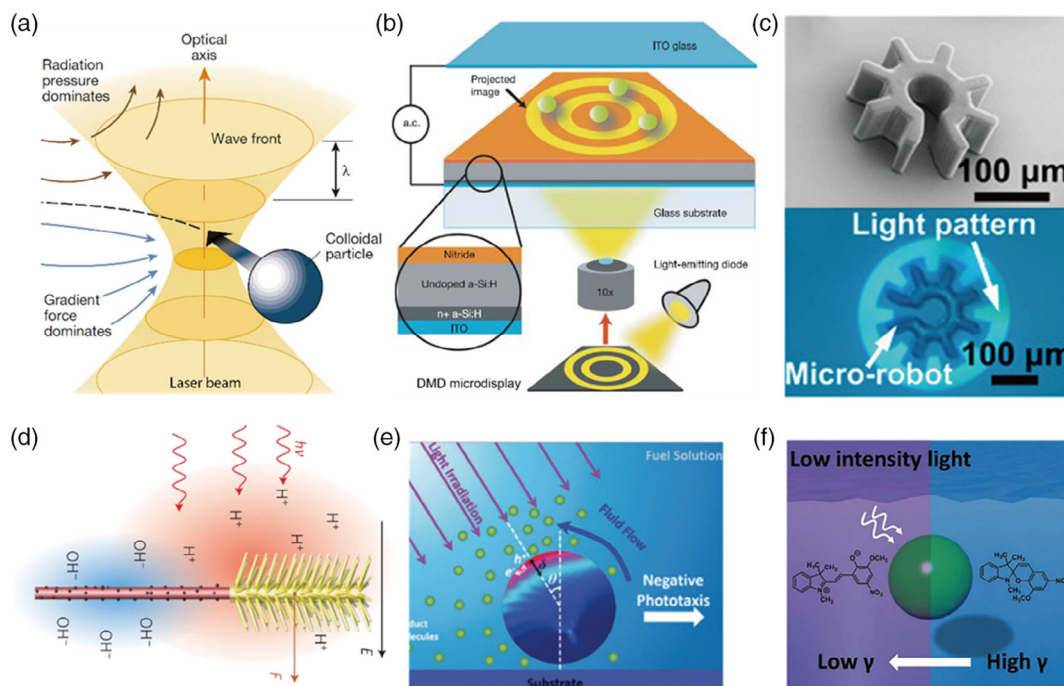
Figure 2. Spatial encoding of light for micro/nanoparticle manipulation. a) Schematic of optical tweezers using a strongly focused light beam to trap particle. Reproduced with permission.[107] Copyright 2003, Nature Publishing Group. b) Schematic of optoelectronic tweezers using a patterned light field. Reproduced with permission.[42] Copyright 2005, Nature Publishing Group. c) SEM image of a cogwheel-shaped microrobot and its operation by a structured light field. Reproduced with permission.[43] Copyright 2019, The National Academy of Sciences of the USA d) Schematic of a tree-like LMNR, which can be navigated via shadowing effect. Reproduced with permission.[47] Copyright 2016, Nature Publishing Group. e) Phototactic motor made of simple TiO_2 microsphere. Reproduced with permission.[48] Copyright 2017, Wiley-VCH. f) Schematic of liquid micromotor showing positive phototaxis due to the photochromism and interfacial surface tension changes. Reproduced with permission.[51] Copyright 2018, The Royal Society of Chemistry.

Most recently, a polarotactic LMNR was demonstrated using Sb_2Se_3-ZnO core-shell nanowires (**Figure 3**a),[56] therein the covalently bonded 1D $(Sb_4Se_6)_n$ chain in Sb_2Se_3 crystalline

nanowire provided a sufficient dichroic absorption of orthogonally polarized light relative to the <001> direction. Such a dichroism effect helps steer a microswimmer assembled by
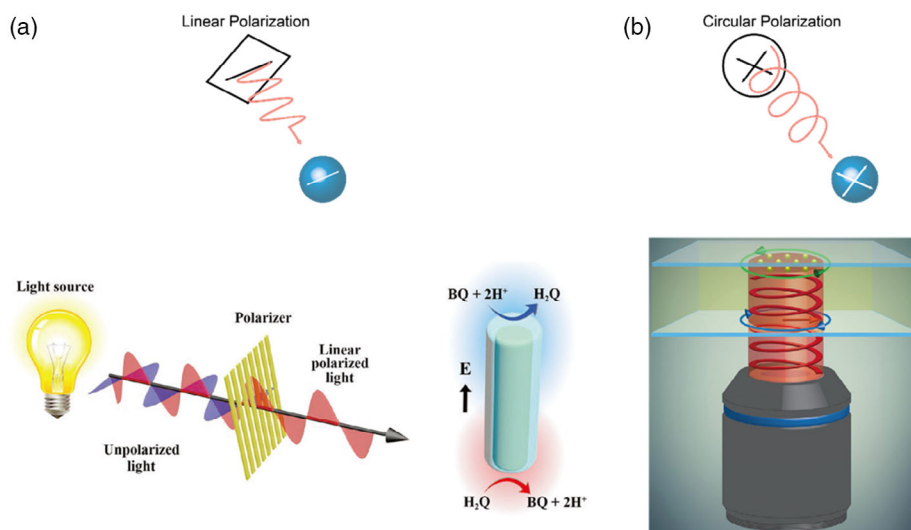

Figure 3. Polarization-based encoding modes and related studies. a) Polarotactic Sb_2Se_3-ZnO core-shell nanowire LMNR via the interaction of linearly polarized light. Reproduced with permission.[56] Copyright 2019, Wiley-VCH. b) Rotation of silver nanoparticles array by a circularly polarized laser beam. Reproduced with permission.[59] Copyright 2018, Nature Publishing Group.

two LMNRs, allowing LMNR navigation by polarization direction of light.

Other than the linearly polarized light, circularly polarized light, in principle, could also be utilized if materials with substantial circular dichroism (CD) are adopted in LMNR. In contrast to linearly polarized light, the polarization direction of circularly polarized light is not affected by the scattering media such as living tissues, which is particularly suitable for the application in noninvasive nanosurgery. However, as most materials and structures only show minuscule ellipticity (θ) or CD values (usually from tens to hundreds of mdeg),[57,58] a microswimmer navigated by circularly polarized light is challenging at this stage. Some recent successes have been achieved in the optical tweezers system to realize the controlled rotation of plasmonic scattering materials (Figure 3b).[59] The rotation direction of the silver nanoparticle array highly depends on the array size as a result of the flip of torque direction. It can be envisioned that a better understanding of chiral molecules and metamaterials may offer more knowledge for the discovery and design of novel LMNRs,[60] which may support the navigation of LMNRs by circularly polarized light. Another possible method to overcome the intrinsic low CD limitation of materials is to incorporate quarter waveplate thin film into existing LMNR.[61] The waveplate converts the circularly polarized light into linearly polarized light, facilitating differentiation between different circular polarization states.

2.3. Frequency Encoding Mode for LMNRs

In optical communication, light with different colors/wavelengths can spontaneously transport through an optical fiber, which offers wavelength domain multiplexing communication. Similarly, the frequency-dependent actuation of LMNRs can also be achieved with spectrum-selective materials, which enabled the selective addressing of LMNRs. To give an overview of existing LMNRs from the perspective of frequency, we will first revisit the representative LMNRs driven by UV, visible, and near-infrared (NIR) light, followed by the discussion about the emerging LMNRs operated under radiofrequency and X-ray waves. After that, the studies on frequency-selective actuation will be discussed.

For UV light, the incident photons absorbed by LMNR with asymmetric structure usually first initiate photoelectrochemical reactions (**Figure 4**a).[62] Then the nonuniformly distributed reaction products propel the LMNR through diverse phoretic mechanisms. However, the UV light is not preferred for biological applications due to the potential damage to tissue and insufficient penetration depth, which encouraged the development of LMNRs powered by visible and NIR light via self-electrophoretic or photothermal effects (Figure 4b–d).[20,23,63–67] Notably, the LMNR made of core-shell p-n junction silicon nanowire operate under both visible and NIR illuminations.[20] By engineering the photonic structure and the optical resonance inside this
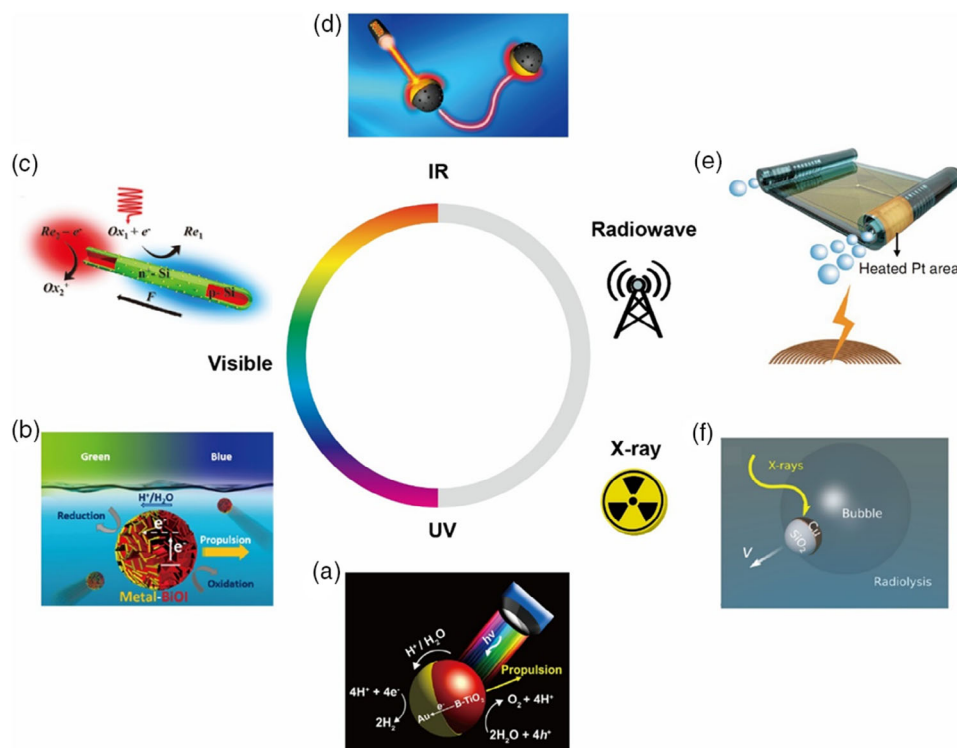

Figure 4. LMNRs driven by incident electromagnetic waves with diverse frequencies. a) Au/TiO$_2$ Janus micromotor which can be operated under UV and visible light. Reproduced with permission.[62] Copyright 2017, American Chemical Society. b) BiOI-metal Janus micromotor propelled in pure water under visible light. Reproduced with permission.[63] Copyright 2017, American Chemical Society. c) Visible−NIR light-driven LMNR built from core-shell p-n junction silicon nanowire. Reproduced with permission.[20] Copyright 2017, Wiley-VCH. d) Au/silica Janus micromotor that can be photothermally driven by NIR light. Reproduced with permission.[23] Copyright 2016, American Chemical Society. e) Flexible motile microsystem driven by radiofrequency wireless power. Reproduced with permission.[68] Copyright 2020, Nature Publishing Group. f) Cu/SiO$_2$ Janus micromotor that can be driven by X-ray. Reproduced with permission.[69] Copyright 2017, American Chemical Society.

nanowire, the wavelength-dependent light absorption and thus motion speed can be observed.

In principle, all electromagnetic waves can be used to power LMNRs, whereas some wavelengths, such as X-ray for computerized tomography, terahertz (THz) wave for THz imaging, and radiowave for magnetic resonance imaging, have been widely applied in medical scenarios, which promised the use of LMNRs for biomedical applications. For instance, a submillimeter motile twin-jet-engine microsystem (MTJEMS) was recently developed with the wireless power at radiofrequency ($\approx$3.5 kHz, Figure 4e).[68] This highly integrated platform combined power collection and multifunctional components (e.g., propelling engine, an optoelectronic device, actuator) as a whole, moving a step toward microrobots with complex onboard circuits and decision-making ability. On the other side, Xu et al. proposed a Cu/SiO$_2$ Janus micromotor, which can be driven by the X-ray at 6.3 keV (Figure 4f).[69] The H$_2$ produced by radiolysis at the Cu site is responsible for the translational motion. Also glycerol and acrylamide need to be added for stabilizing particle and reducing by-products of water radiolysis, respectively.

With the broad frequency range from radiowave to X-ray, the better controllability of LMNR can be realized. The operator can selectively address individual LMNR or program a variety of actions using light with different frequencies. An asymmetric micromotor was proposed with different caps that can resonate at distinct frequencies (**Figure 5**a).[70] Using corresponding incident light, the motion direction can be selected via thermophoretic drift. Moreover, the hybridization of semiconductors with different bandgaps can bring in varied motive behaviors under different illuminations (Figure 5b).[71] Such results suggested the possibility of building monolithic LMNR by rationally assembling frequency-responsive modules.

A next relevant question is how much tunability can be realized, regarding the operation frequency of LMNR, which will limit the degree of freedom for manipulation. As a pilot study, core-shell Zn$_X$Cd$_{1-X}$Se-Cu$_2$Se nanowires were shown for its continuously tunable bandgap due to the controllable alloying between ZnSe and CdSe.[72] Given the abrupt absorption

cut-off at the band edge, the motion of LMNRs can be differentiated by switching the wavelength of the incident light. With the help of distinctive material absorptions, the independent manipulation of individual LMNRs via nonoverlapping frequency channels can be realized. Recently, Zheng et al. reported a Janus TiO$_2$/Si nanotree LMNR that can be orthogonally controlled with blue and red light (Figure 5c).[73] This intriguing capability originated from the organic dye sensitizing of TiO$_2$, which endowed the LMNR with wavelength-selective light absorption. Overall, these studies heralded the exciting applications, such as microsurgery and manufacturing at nanoscale, by deploying a swarm of coordinated LMNRs with independent actuation.

3. LMNRs with Hybrid Encoding Modes Beyond Light

Alongside the light encoding modes discussed in the previous sections, the hybridization between light and magnetic, acoustic, or electric fields substantially enriched the functionality of LMNRs and sparked a multitude of studies from both fundamental and application aspects. Among these hybrid encoding modes, the light–magnetic mode has been most extensively explored.[74–79] The outstanding advantage of this mode is the synergy of the precise steering by the magnetic field and the efficient propelling by photochemical reactions. For instance, the peanut-shaped Fe$_2$O$_3$ LMNR succeeded in tracing, capturing, transporting, and releasing a cargo many times the size of the microrobot (**Figure 6**a).[74] The facile fabrication required by the functioning components for light and magnetic field brought about diverse LMNRs (Figure 6b),[75] offering more design space for LMNRs.

Resembling the magnetic field, the acoustic field is also compatible with biological applications and can help guide LMNRs to approach the target object. By exploiting the acoustic field, Wang et al. accurately poked an Au-coated tubular LMNR against a Hela cell (Figure 6c).[4] The presence of NIR light boosted the perforation with additional photothermal force, meeting the demand for the cell membrane penetration that is 40 times larger than the
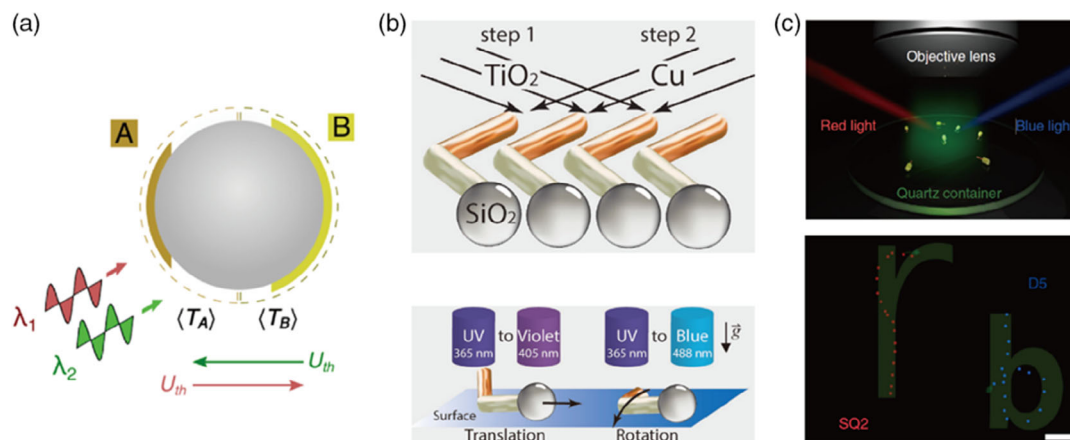

Figure 5. LMNR manipulation by frequency-selective encoding. a) Micromotor based on polystyrene particle, with caps resonant at different wavelengths, can maneuver the motion direction through thermophoresis. Reproduced with permission.[70] Copyright 2016, American Chemical Society. b) Multicomponent microswimmer that exhibited dissimilar behaviors under different incident light wavelengths. Reproduced with permission.[71] Copyright 2018, Wiley-VCH. c) Janus TiO$_2$/Si nanotree motor with multichannel controllability by orthogonal dye sensitizing. Reproduced with permission.[73] Copyright 2017, Nature Publishing Group.
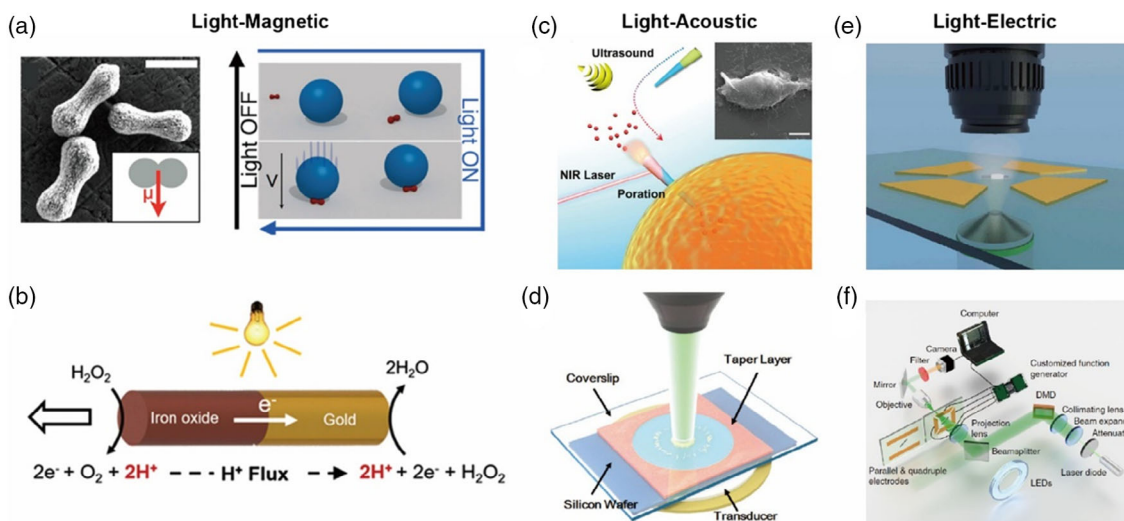
Figure 6. Representative LMNRs encoded by hybrid modes. a) Peanut-shaped hematite LMNRs propelled by photochemical reaction and steered by an external magnetic field. Reproduced with permission.[74] Copyright 2013, American Chemical Society. b) Au-Fe₂O₃ motor driven by light-induced self-electrophoretic movement with magnetic steering. Reproduced with permission.[75] Copyright 2017, Royal Society of Chemistry. c) Cell poration by the acoustic and NIR photothermal force of LMNR. Reproduced with permission.[4] Copyright 2019, American Chemical Society. d) Nanomotor "firework" created by the cooperative effect of light and acoustic fields. Reproduced with permission.[80] Copyright 2018, Wiley-VCH. e) Visible light-gated reconfigurable electric nanomotor. Reproduced with permission.[82] Copyright 2018, The Authors, some rights reserved; exclusive licensee American Association for the Advancement of Science. Distributed under a CC BY-NC 4.0 License. f) Light-encoded silicon nanowire stepper motor in an electric field. Reproduced with permission.[81] Copyright 2019, Nature Publishing Group.

acoustic driving force. Moreover, combining the light and acoustic fields may also lead to novel swarming behaviors of LMNRs. The smart aggregation of nanomotors at the pressure node in the acoustic field and its perturbation by optical radiation force created a "firework" of the Au cluster (Figure 6d).[80] More importantly, this technique can be universally applied to a series of nanomotors (Au, Pd, and polypyrrole), with the immunity to high ionic strength media, facilitating its application in salty biofluids.

Last but not least, by incorporating the long-established Maxwell–Wagner interfacial polarization effect and the electrical double layer (EDL) charging effect, a visible light-gated electric rotor was demonstrated by Liang et al. (Figure 6e), which showcased the light–electric hybrid manipulation.[81] Upon light illumination, the photoconductivity of the silicon nanowire can be modulated, which reconfigured the interaction between the polarized nanowire and the external AC electric field, controlling the acceleration, deceleration, stopping, and reversal rotation of LMNR (Figure 6f).[82] The prompt switch of nanomotor by light enabled the words expressing in Morse code. By constructing the structural light field with DLP system, multiple light–electric stepper motors can be independently controlled under the same E-field. This study exemplified the hybridization of advanced encoding modes for LMNR manipulation, opening an avenue to new hybrid encoding modes for LMNRs.

4. Assembly and Swarming Behaviors of LMNR Systems

Due to their limited sizes and simple structural designs, most MNRs are unlikely to realize sophisticated functions individually. On the other hand, macroscopic robots usually bear advanced functions through the designed assembly of multiple simple components. Inspired by the paradigm of macroscopic robots, the assembly of many simple MNRs could be a viable approach toward micro/nanomachines and intelligent nanorobotic systems. In this direction, a new set of techniques will be needed to control, manipulate, and assemble multiple MNRs into functional structures. In addition, the interactions between MNRs could lead to the dynamic assembly of MNRs (MNRs swarming or schooling). Swarming behaviors are ubiquitous in nature, such as schooling of fishes, flocks of birds, and bacterial colonies.[83–85] As the artificial counterparts, the colloidal particles, including active and passive ones, were recently designed to mimic the swarming behaviors in nature. Benefiting from the development of the highly controllable single MNR,[3,14,17,86,87] a large inventory is available for advanced intelligent colloidal systems beyond single MNR.

To date, varieties of stimuli, such as chemical gradient, magnetic field, electric field, ultrasound as well as light, have been successfully used for the assembly and swarming of MNRs.[88–92] Notably, the light-manipulated system has lately been explored due to its multi-encoding modes, on-demand wireless operation, and excellent spatial and temporal controllability.[1,3,5] In principle, light-controlled assembly and swarming can be categorized into two major groups according to driving mechanisms: 1) photochemical reaction and (2) photoinduced physical field. Here, we will first illustrate the two mechanisms and then discuss the related applications correspondingly.

4.1. Photochemical-Reaction Related Assembly and Swarming of LMNR Systems

With the energy from the photons, light can drive diverse photochemical reactions, such as photocatalytic, photolytic, and

photoisomerization reactions, which further produce ions, molecules or lead to molecular conformation change to drive the colloidal system. A typical process of photochemical reaction is shown in **Figure 7**a. The light-triggered chemical reaction produced an ion gradient and created a localized electric field due to the different diffusion rates of anions and cations.[88,93] The motion of particles is dominated by the electrophoretic propulsion and the electro-osmosis flow from the substrate, in which the swarming behaviors of particles are primarily governed by the electro-osmosis flow to push the particles closer

or away from each other. For example, silver chloride (AgCl) is a typical photolytic material and has been widely exploited in the photography industry due to its photosensitivity. Under UV light illumination, the photolytic reaction at pH = 5 proceeds as[94]

$$4AgCl + 2H_2O \xrightarrow{h\nu,\ Ag^+} 4Ag + 4H^+ + 4Cl^- + O_2 \qquad (1)$$
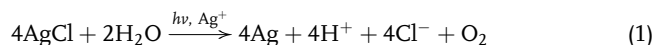
Due to the fast diffusion of H^+, an inward electro-osmosis flow was established near the glass substrate, which
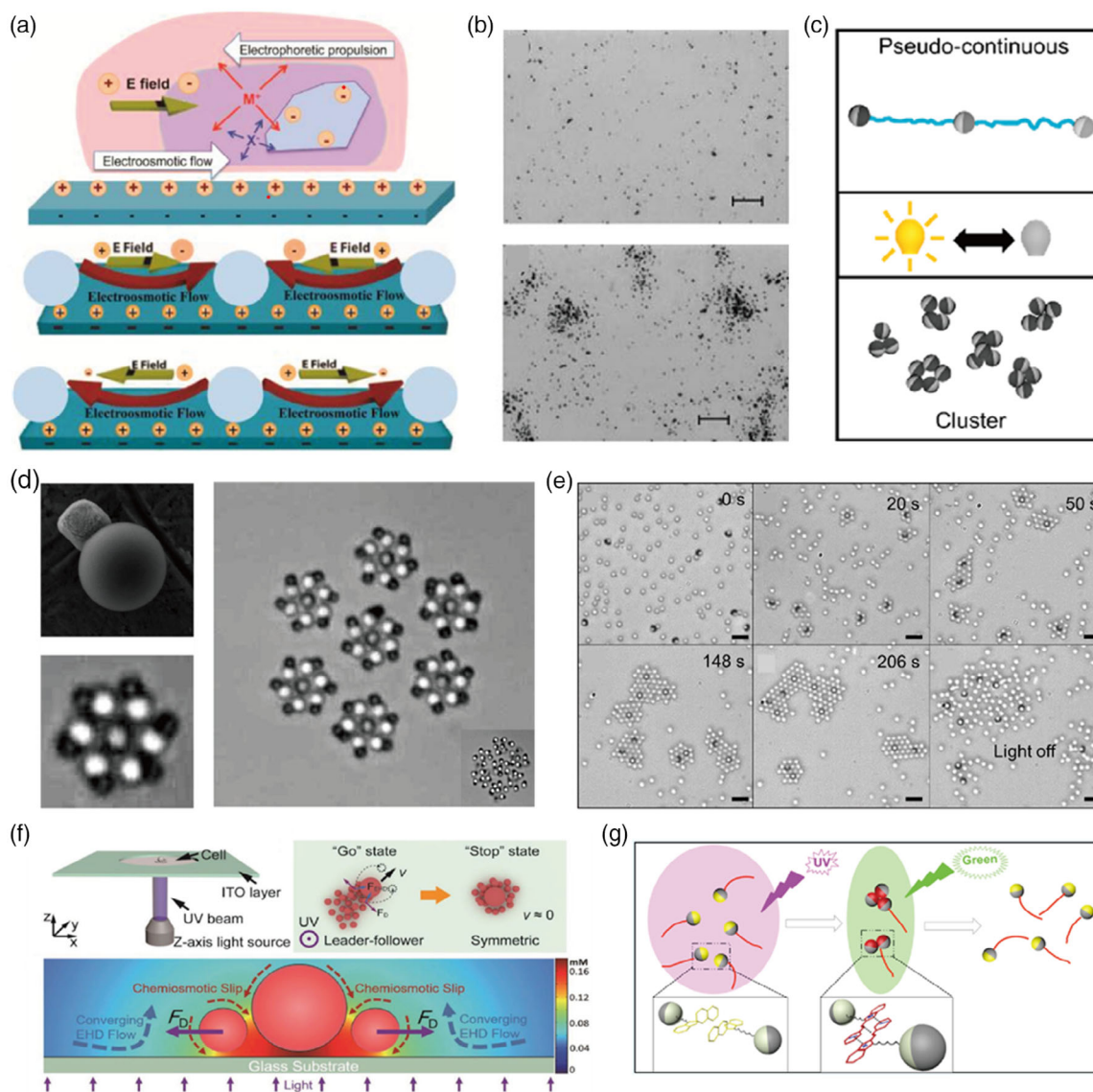

Figure 7. The mechanism and demonstrations of chemical-reaction related LMNR swarming systems. a) Schematic of the diffusiophoresis mechanism. The interaction of particles depends on the relative diffusivities of the cations and anions. Reproduced with permission.[88] Copyright 2015, American Chemical Society. b) Schooling behavior of AgCl particles under UV light illumination. Reproduced with permission.[94] Copyright 2009, Wiley-VCH. c) Different swarming behaviors of Ag-based oscillating micromotors by temporal control. Reproduced with permission.[96] Copyright 2020, American Chemical Society. d) Hierarchical assembly of self-spinning rotors controlled by the spatiotemporal light patterns. Reproduced with permission.[101] Copyright 2018, Nature Publishing Group. e) Light-controlled crystal formation in a mixture of TiO₂–SiO₂ Janus micromotors and SiO₂ passive particles. Reproduced with permission.[102] Copyright 2017, Wiley-VCH. f) Schematic of hierarchical microswarms with multimode behaviors in response to light signals. Reproduced with permission.[105] Copyright 2020, Wiley-VCH. g) Schematic diagram of light-controlled assembly with spiropyran-modified SiO₂–Pt Janus micromotors. Reproduced with permission.[106] Copyright 2015, American Chemical Society.

assembled the particles while avoiding contact between particles into clusters. As shown in Figure 7b, the reversible exclusion/schooling can be triggered by UV light. Similarly, based on the self-diffusiophoresis mechanism, the swarming behavior was observed in SiO_2–TiO_2 Janus particle as well as Ag_3PO_4 particle systems.[21,95] Recently, Wang and co-workers systematically studied the temporal control of Ag-based photoactive micromotors. By tuning the oxidation of silver and photodecomposition of AgX, different modes of oscillating traveling waves were observed. Interestingly, the nonoscillatory micromotors can be transformed into spontaneous oscillators after the diffusion and deposition of Ag ions, which shows an intelligent "teaching and learning" behavior and the possibility of smart LMNR design (Figure 7c).[96–99]

An artificial active system can be achieved by the light-triggered assembly. Palacci et al. have, for instance, demonstrated a crystal formation in photoactivated Fe_2O_3-polymer sphere (3-methacryloxypropyl trimethoxysilane) patchy particles, which were referred to as "living crystals", and showed reversible crystallization and disassembly manipulated by light.[100] With the same active particles, the phototactic swimmers can be assembled into self-spinning microgears under a focused laser beam, as shown in Figure 7d.[101] On top of that, the co-rotating rotors can further cooperate to hierarchically constitute the synchronized gears of a micromachine. Recently, Singh et al. showed a dynamic assembly system by combining active and passive particles, demonstrating that the self-propelled colloids can help build the large scale 2D assembly of the passive particles.[102] Under UV light illumination, light-activated TiO_2/SiO_2 Janus particles serve as the active cores for the nucleation of passive particles (Figure 7e), which is reversible when the light is turned off, resembling the crystal melting due to Brownian diffusion. Similarly, Guan and co-workers reported a system of photocatalytic TiO_2–Pt Janus MNRs, which can control the assembly behaviors of surrounding MNRs or passive colloidal particles through regulating the intensity and pulsed/continuous mode of UV light.[103,104] As a universal strategy, this active-particle-induced assembly can be widely applied to various charged colloidal particles. In addition, the same group recently designed a leader–follower-like active–passive particle system, and multimode swarming behaviors were demonstrated in response to light signals.[105] As shown in Figure 7f, with vertical UV illumination, the photoresponsive followers tend to surround the leader. The asymmetric assembly then gradually grows into symmetric cluster and stops the migration. Moreover, with the sidewise UV signals, positive or negative phototaxis of the swarms can be well controlled by the intensity of light.

The photoactive molecules, like azobenzenes and spiropyrans, can be used to tune the interaction between MNRs, which is an alternative approach to achieve the controllable assembly. For instance, spiropyran and its derivatives exhibit reversible ring-opening/-closing photoisomerization between the spiropyran form and the merocyanine form upon UV or visible light illumination. Ren and co-workers developed spiropyran functionalized SiO_2–Pt Janus catalytic MNRs, which showed light-controlled reversible assembly behaviors.[106] As shown in Figure 7g, under UV light illumination ($\lambda = 365$ nm), spiropyran moieties on the

surface changed to merocyanine isomer, resulting in the dynamic self-assembly of micromotors. As the merocyanine isomerized back to spiropyran form under green light ($\lambda = 520$ nm), the assembly quickly dissociated back to the micromotor monomers.

4.2. Photoinduced Physical-Field-Driven Assembly and Swarming of LMNR Systems

Optical tweezers and photothermal effects have been exploited for the manipulation and assembly of colloidal particles based on the photoinduced physical fields. As discussed in Section 2, the optical force includes two components: a gradient force in the direction of the light intensity gradient and a scattering force in the direction of light propagation.[107–109] Colloidal particle can be drawn along the intensity gradient in the converging beam and trapped near the focal point. With the highly controllable optical force, a variety of organized colloidal patterns have been demonstrated.

Large-scale patterning has been realized by creating optical traps on a patterned substrate, as shown in **Figure 8**a.[110] A 2D plasmonic array was created by a 2D square lattice of gold nanostructures on the indium tin oxide (ITO) glass. Under a Gaussian beam illumination, the colloidal particles can be guided, trapped, and arranged in the periodic plasmonic potential. Moreover, the multiple particles can accumulate in the central region and form predominant (hexagonal) closely-packed structures. After turning off the laser illumination, the particles could disassemble and escape from the array. Similarly, a light-assisted template technique was also utilized for the nanoparticles self-assembly.[111] As shown in Figure 8b, an array of optical traps can be created by exciting a guided-resonance mode of a photonic-crystal slab with 1.55 μm laser, the optical force arising from a strong electric-field gradient near the slab surface attracted the nanoparticles, resulting in an assembled nanoparticle array.

Although the optical tweezers are common and versatile techniques for colloidal manipulation and assembly, the requirement for tightly focused laser beam with precise alignment is a challenge for some applications. The photothermal effect is another effective approach for the manipulation of swarming systems, which dramatically reduced the required light intensity. Although the detailed physical picture of thermophoresis in liquid media is still elusive, the apparent thermophoresis ability of colloidal particles can be quantified by Soret coefficient (S_T), which is defined by $D_T = S_T D$, where D_T is thermophoretic mobility.[22,112–114] Depending on the sign of S_T, particles can migrate along or against the temperature gradient. As shown in Figure 8c, tracer particles accumulated around large particles with positive Soret coefficient due to the upward slip flow, whereas the tracer particles were depleted from the large particles with a negative Soret coefficient.[112] Based on the photothermal effect, Lin et al. reported plasmonic nanoparticles that can be reversibly assembled under reduced power intensity (≈ 10 kW cm^{-2}) by thermophoretic migration of nanoparticles and the enhanced local electric field of the plasmonic substrate.[115] Subsequently, the same group developed a versatile technique, termed opto-thermophoretic
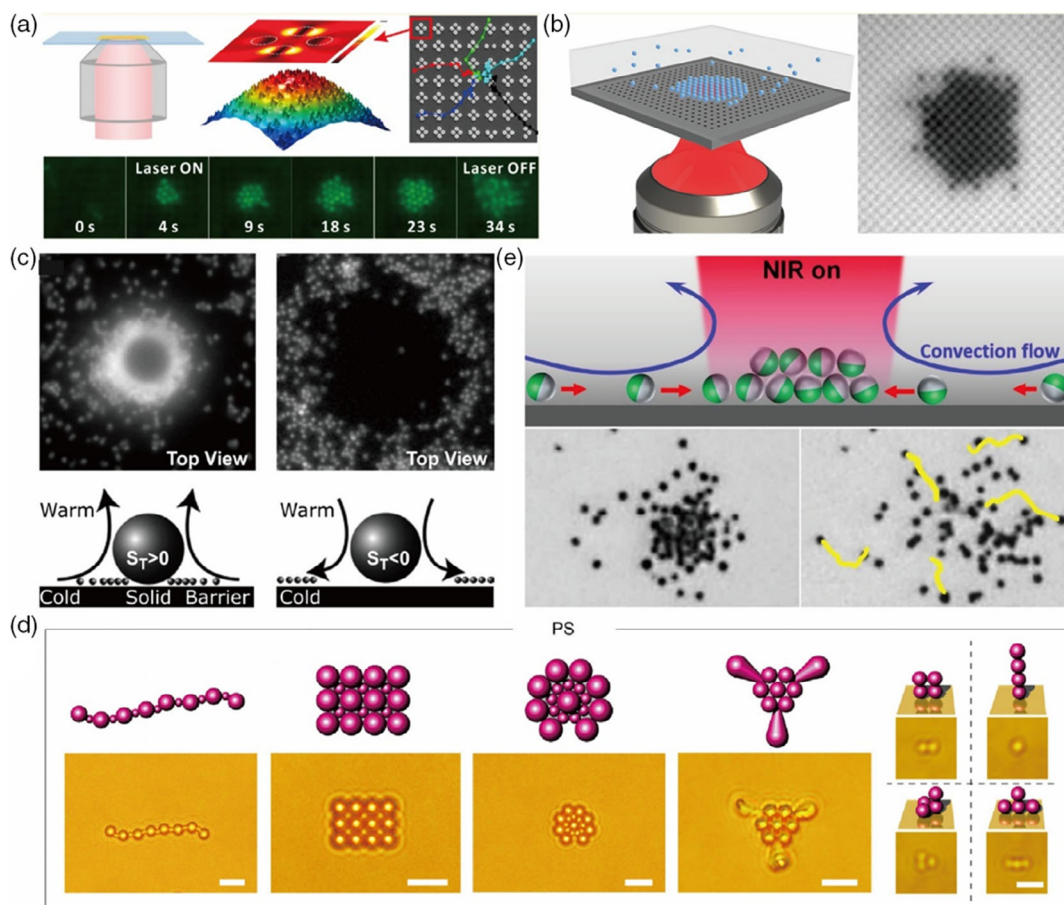
Figure 8. Optical force and photothermal effect-triggered assembly and swarming of LMNR systems. a) On a designed optical lattice, a Gaussian beam at a wavelength of 980 nm can excite surface plasmon resonance and attract the nanospheres to the central region. Reproduced with permission.[110] Copyright 2013, American Chemical Society. b) Schematic and demonstration of light-assisted assembly of PS nanoparticles on a photonic-crystal slab. Reproduced with permission.[111] Copyright 2013, American Chemical Society. c) Schematic and demonstration of attracting/repelling phenomenon, which is determined by the temperature gradient and the Soret coefficient of the large particle. Reproduced with permission.[112] Copyright 2008, American Physical Society. d) OTA and manipulation of 1D, 2D, and 3D structures of PS beads. Reproduced with permission.[116] Copyright 2017, The Authors, some rights reserved; exclusive licensee American Association for the Advancement of Science. Distributed under a CC BY-NC 4.0 License. e) NIR light-induced convection flow for the swarming of micromotors and swarming migration. Reproduced with permission.[117] Copyright 2018, Elsevier.

assembly (OTA), to assemble colloidal particles under a light-induced temperature gradient.[116] The spatial separation of ions with different sizes and solvation energies under the temperature gradient generated a thermoelectric field to drive the charged colloids. As shown in Figure 8d, applying an anionic surfactant cetyltrimethylammonium chloride as the surface charge source, various 1D, 2D, and 3D assembly can be generated. Moreover, due to the general applicability, the OTA strategy can be applied to diverse colloidal sizes and materials. Recently, Guan and co-workers developed another general strategy to create colloidal swarms by photothermal-induced convection flows.[117] Figure 8e shows that the NIR light-induced convection flows dragged the particles to the convection center, and the generated assembly can be well controlled by simply moving the NIR spot. This facile strategy can be used for various micromotors as well as microorganisms regardless of the geometry and material, showing great potential for LMNRs designs and applications.

4.3. Representative Demonstrations of LMNRs Assembly and Swarming

As we have stated, sophisticated functions are not expected for individual MNR, while the assembly and swarming systems (swarmbot) may be the most promising way toward an intelligent MNR system. To date, intelligent micro/nano swarmbot has not yet been achieved, whereas some light-controlled assembly has been demonstrated, which could be the first step toward the target.[118]

By creating patterned illumination, a corresponding pattern can be transferred to the distribution of LMNRs due to phototaxis, induced phoretic flow, or surface chemistry. As shown in **Figure 9**a, Fe_2O_3 nanoparticles escaped from the illuminated zone to form the pattern of "HIT" due to the light-induced electrolyte diffusiophoresis. This strategy can be extended to create large-scale complex shapes assembled by motors with well-defined boundaries. In addition, Sun et al. developed a
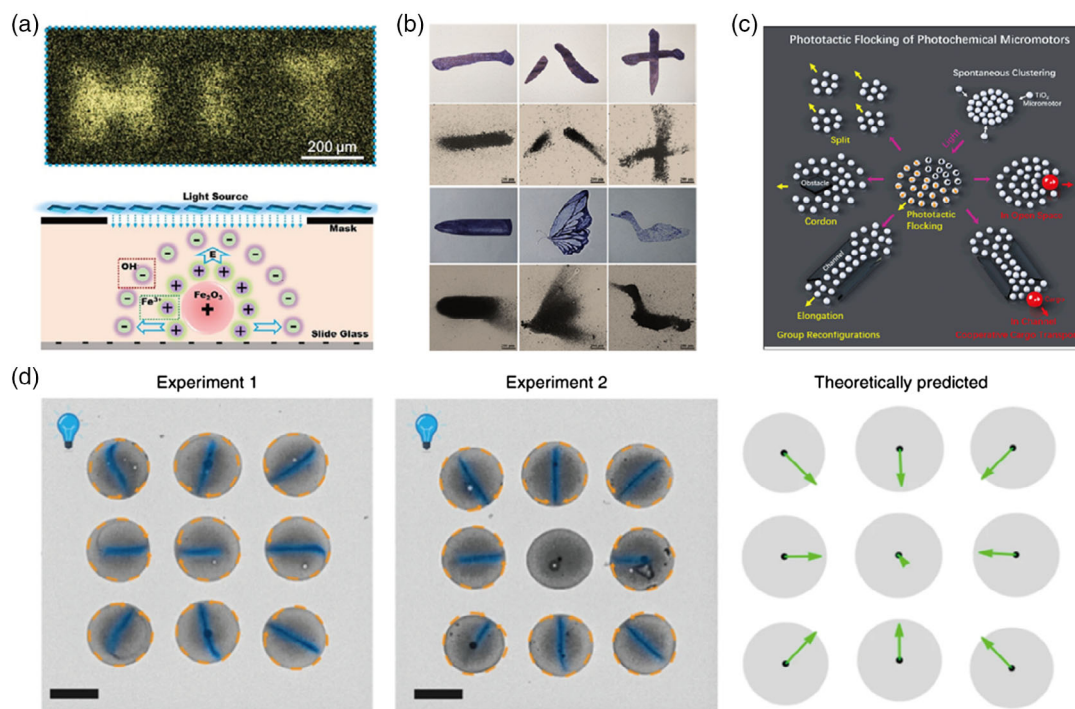
**ADVANCED
SCIENCE NEWS**

www.advancedsciencenews.com

**ADVANCED
INTELLIGENT
SYSTEMS**
Open Access

www.advintellsyst.com

Figure 9. Representative LMNR swarming systems. a) Schematic and demonstration of microstructure formation by the light-induced self-assembled pattern of Fe_2O_3 nanomotors. Reproduced with permission.[118] Copyright 2019, Wiley-VCH. b) In-solution calligraphy and painting by controllable aggregation of PS@PDA micromotors. Reproduced with permission.[119] Copyright 2019, American Chemical Society. c) Schematic illustration of phototactic flocking of photochemical micromotors and the application for cargo transport. Reproduced with permission.[120] Copyright 2019, Cell Press. d) Alignment of the flow directors for arrays with high symmetry. The scale bars correspond to 150 μm. Reproduced with permission.[121] Copyright 2020, Nature Publishing Group.

NIR light-driven dynamic swarming system using polystyrene microspheres and polydopamine core-shell (PS@PDA) micromotors.[119] Due to the reversible hydrogen bonding and π–π stacking interactions between the adjacent PS@PDA micromotors, the micromotor aggregation can be tuned by the shape of illumination, leading to in-solution calligraphy and painting as shown in Figure 9b. Recently, Mou et al. reported that hydroxyl functionalized TiO_2 micromotors could flock in aqueous media through electrolyte diffusiophoresis, which can be controlled by the pulsed light navigation and cooperatively transport large cargoes (Figure 9c).[120]

One the other hand, the self-organization of active particles under illumination is of great interest in complex science and dynamic systems. Recently, Singh et al. reported a light-driven symmetry breaking and the emergence of self-organized patterns with chemically active particles that exhibit negligible motility by themselves.[121] As shown in Figure 9d, titania powder particles with negligible self-propulsion were confined in a sessile water droplet containing hydrogen peroxide, which was further immersed within a thick film of silicone oil. Under the illumination of UV light, the uniformly distributed particles exhibited a transition to collective motion, leading to self-organized flow patterns. More interestingly, a collection of active drops showed long-ranged ordering of the flow patterns, due to the chemical communication between droplets.

With the development of simple swarming systems, the next step is the exploration of nontrivial collective emergence. As described in the book "*Emergence: The Connected Lives of Ants, Brains, Cities, and Software*",[122] the complex ant colony is constructed by the individual ant with only several discrete actions, while the colony exhibits high-level intelligence. The collective intelligence emerges from the large networks of lower-level actions of the ants. As the counterparts, the artificial swarming system of MNRs offers a perfect model for the study of self-organizing behaviors and the "bottom-up" revolution in the biological world and social behavior.

5. Challenges and Outlooks for Biomedical LMNRs

In view of the aforementioned advantages of LMNRs, many intriguing demonstrations have emerged in recent years, ranging from environmental remediation,[103,123–127] cargo delivery[48,74,128–130] to biomedical-related manipulations.[35,78,131–133] However, for the implementation of LMNRs in healthcare, several critical challenges, including ion tolerance, supporting chemical toxicity, propulsion efficiency, and biofouling,[1,5,134,135] still impeded the full realization of their potential. Although the applications for LMNRs are broad, the biomedical application is still the most desired target. Therefore, in this section, we summarize the advanced manipulations achieved so far and discuss the potential solutions to the most urgent challenges for the biomedical application of LMNRs.

5.1. Advanced Manipulations of LMNRs

5.1.1. LMNRs Manipulation for Biomedical Application

The biomedical application is one of the most alluring areas for LMNRs. Novel LMNRs hold promise to enhance the efficacy of existing light-based modalities, such as photothermal therapy (PTT),[136,137] and photodynamic therapy (PDT).[138,139] Currently, NIR-based LMNRs were intensively investigated due to their appealing biocompatibility and penetration depth across living tissues.

The NIR LMNRs are normally operated by thermophoretic mechanism when a temperature gradient is created across the LMNRs. For instance, Xuan et al.[140] reported Janus mesoporous silica nanomotor modified with macrophage cell membrane cloaking for active cancer cell seeking and thermomechanical cell membrane percolation. Recently, Jiao et al. designed gold half-coated mesoporous silica as a nanocarrier.[132] This Janus nanocarrier was propelled by NIR irradiation, where the thermomechanical force can percolate the cytomembranes. Moreover, this nanocarrier was designed to respond to reactive oxygen species (ROS) in the cellular environment to improve the drug delivery efficacy. As shown in **Figure 10**a, after the penetration into the tumor cell, the mesoporous silica responded to ROS in the tumor cell and changed from hydrophobic to hydrophilic, which further triggered drug release. Moreover, Janus hollow mesoporous TiO_2/Au microswimmers triggered by UV light were also developed as active drug carriers,[78] in which the anticancer drug (doxorubicin) was loaded into the mesoporous structure for active drug delivery. In addition, an optically driven micromotor was demonstrated to manipulate axonal growth.[35] As shown in Figure 10b, a birefringent vaterite particle can be trapped and spun by circularly polarized light. The localized microfluidic flow caused by particle spin generated a shear force to guide the growth of axon.

5.1.2. LMNRs for Cargo Delivery

As a nanomachine, artificial LMNRs can be precisely controlled to capture, transport, and release cargos. Several pioneering studies on cargo transportation by LMNRs have been reported. Palacci et al. reported a colloidal hematite docker propelled by photocatalytic decomposition of H_2O_2 and steered by an external magnetic field.[74] As shown in Figure 10c, the cargo with negative diffusiophoresis can be docked on the hematite particle upon illumination, guided by the external magnetic field, and finally released near the target. Recently, ZnO/Au nanorod was demonstrated for the capability of cargo delivery by tuning two modes of motion (Figure 10d).[141] As discussed in the previous section, isotropic semiconductor nanoparticles (e.g., TiO_2, ZnO, CdS, etc.) can be used as LMNRs due to the shadowing effect.[48] As shown in Figure 10e, LMNRs can capture, transport, and release passive cargoes on demand due to the light-regulated motion and the diffusiophoretic attraction with cargoes. Very recently, a well-defined single-component star-shaped $BiVO_4$ (BVO) micro/nanostructure was introduced as a visible-light-driven micromotor.[128] Passive particles, as well as living microorganisms, can be attracted, transported, and released by

switching the light on/off without specific surface functionalization (Figure 10f). As a result of the highly oxidative radicals photocatalytically generated on the BVO surface, this BVO micromotor also showed fungicidal activity, which may serve as a promising disinfection tool for the removal of microbial contamination in water.

5.2. Challenge: Operation in High Ionic Strength Media

To sense and respond to the surrounding environment, the chemical reaction powered MNRs are preferred as they naturally respond to the surrounding chemical concentrations in solution. However, most chemical reaction powered MNRs are propelled by the self-generated electric field; therefore, their swimming capability is susceptible to the solution salinity. The MNR's ability to swim in high ionic strength media, namely ion tolerance, is a critical requirement for the biomedical application,[5] which was fallaciously regarded as impossible as prevented by fundamental electrokinetics.

Recently, our group discovered that the Debye layer collapsing is not inevitable in high ionic strength solutions. A highly solvated polyelectrolyte coating can effectively support a non-neutral layer outside the particle surface to replace the role of the Debye layer, which improved the ion tolerance of LMNRs. In this case, the surface conductivity through the grafted coating is not negligible, and the self-electrophoresis silicon micromotor was demonstrated, with over 100 times improvement in ion tolerance, to operate in salty solution and diluted body fluid (**Figure 11**a).[142]

Although this new theory is only applicable to MNRs based on self-electrophoresis, the ion tolerance improvement with small hydrodynamic size and hydrated porous coating may be universal for other propulsion mechanisms. For instance, individual enzyme molecules or enzyme-coated nanoparticles showed significant chemotactic migration in a salty environment (Figure 11b).[143–145] Mesoporous urease-powered silica nanomotors were able to self-propel in ionic media (Figure 11c).[146] Polymeric stomatocyte nanomotors migrated at a reduced velocity in H_2O_2/phosphate-buffered saline (PBS) solution.[147] Highly porous BiOI-based Janus micromotor can be propelled at a reduced speed in 1 mM NaCl solution.[63] More recently, the polycaprolactone encapsulated Q.D./Fe_3O_4 LMNR was reported, which can operate in human serum and blood (Figure 11d).[148] Further research would be needed to improve the fundamental understanding of the electrokinetic process at a porous structure surface, which will lead to further improvement in ion tolerance. We believe that conquering this "ion tolerance challenge" will be the key toward more in vivo MNR systems.

5.3. Biocompatible Supporting Chemical and Improved Propulsion Efficiency

Most MNRs require chemical fuels to support the surface reaction and generate propulsion. Unfortunately, the chemomechanical conversion efficiency is extremely low, where high reaction speed is necessary to create sufficient phoretic flow for self-propulsion. As a result, catalysis-based MNRs prefer to use high-energy but toxic chemical fuels such as H_2O_2, N_2H_4,

**ADVANCED
SCIENCE NEWS**

www.advancedsciencenews.com

**ADVANCED
INTELLIGENT
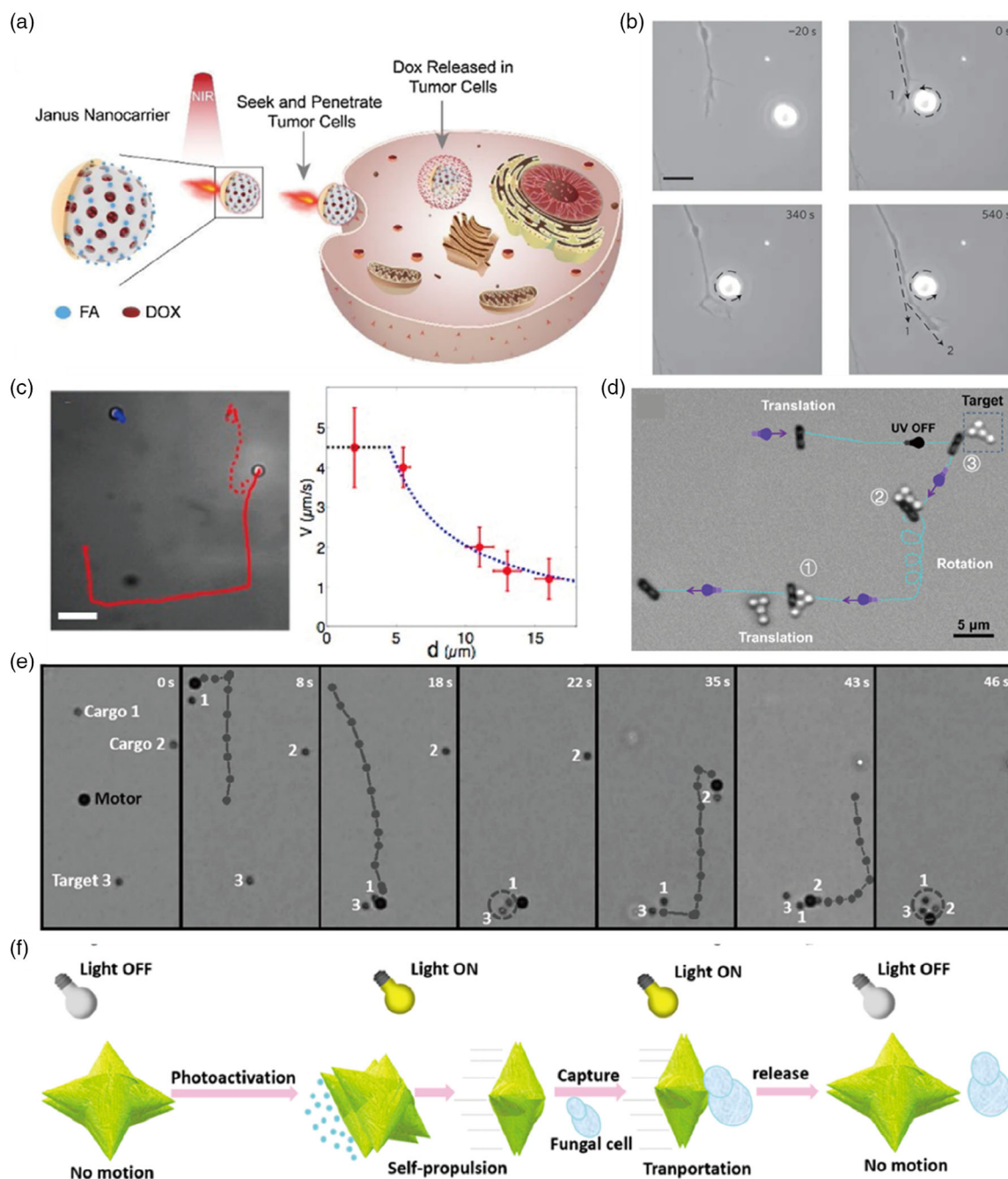SYSTEMS**
Open Access

www.advintellsyst.com

Figure 10. Demonstration of advanced manipulations of LMNRs. a) Illustration of the NIR-powered Janus nanocarrier for the penetration of tumor cell and controlled drug release. Reproduced with permission.[132] Copyright 2020, Elsevier. b) Controllable spinning of the bead trapped by circularly polarized light to manipulate the growth direction of individual axons (nerve fibers). Reproduced with permission.[35] Copyright 2012, Nature Publishing Group. c) Trajectory of a hematite particle steered with an external magnetic field to pick up and dock colloidal cargo. The velocity depends on the cargo diameter. Reproduced with permission.[74] Copyright 2013, American Chemical Society. d) ZnO/Au rod can capture, transport, and release cargos by tuning its translational and rotational motion. Reproduced with permission.[141] Copyright 2020, American Chemical Society. e) Light-controlled TiO$_2$ micromotor was applied for the transport of silica particle cargoes. Reproduced with permission.[48] Copyright 2017, Wiley-VCH. f) Visible-light-driven single-component BiVO$_4$ micromotor for the transportation of microorganisms. Reproduced with permission.[128] Copyright 2019, American Chemical Society.

Br$_2$, and I$_2$,[147,149–153] and to use the most active catalysts to provide the highest reaction rate.

Light, as additional energy input, can help overcome the activation barrier and improve the reaction rate, which provides an alternative route to improve the biocompatibility of MNRs. For example, glucose is an ideal biocompatible fuel due to its abundance in biological fluids, which has been used to drive enzymatic MNRs. Recently, Wang et al. developed a highly
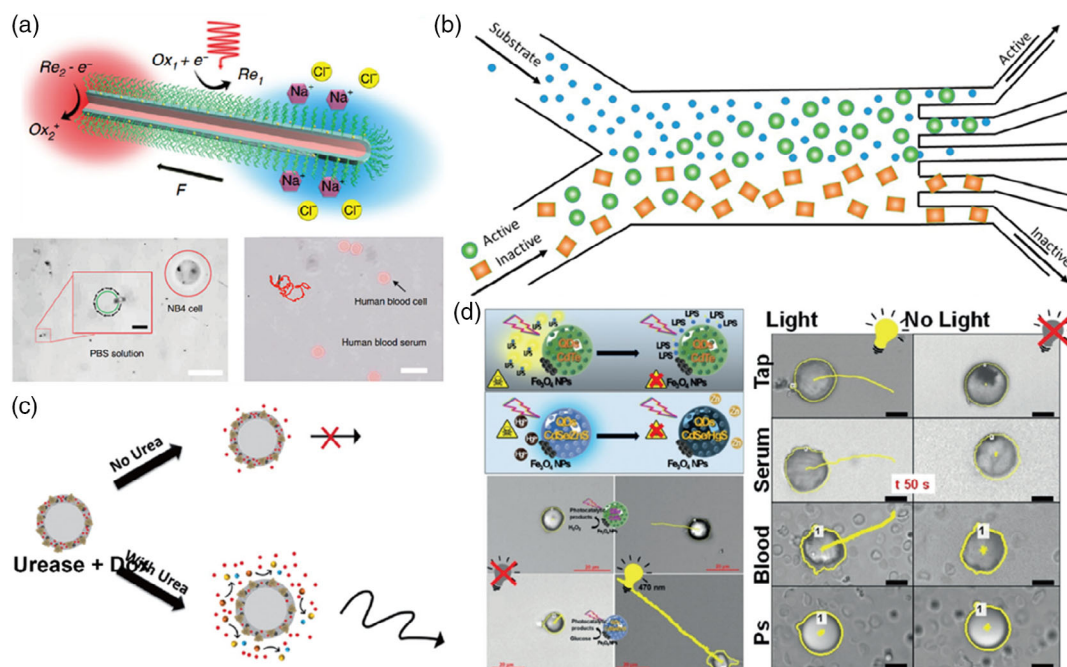
Figure 11. Demonstrations of MNR propulsion in high ionic strength media. a) Enhanced ion tolerance of polyelectrolyte-coated silicon micromotor in biological media. Reproduced with permission.[142] Copyright 2019, Nature Publishing Group. b) Schematic of chemotactic separation of enzymes in PBS buffer. Reproduced with permission.[143] Copyright 2014, American Chemical Society. c) Urease nanobots in PBS buffer for drug delivery. Reproduced with permission.[146] Copyright 2018, Wiley-VCH. d) QD/Fe$_3$O$_4$ encapsulated by biocompatible polycaprolactone polymer as visible-light-driven micromotors in biological media. Reproduced with permission.[148] Copyright 2019, Wiley-VCH.

efficient glucose-fueled cuprous oxide@N-doped carbon nanotube (Cu$_2$O@N-CNT) micromotor driven by visible light (**Figure 12**a).[154] Benefiting from the efficient photocatalytic decomposition of glucose, this LMNR showed high motility comparable to conventional catalytic Janus MNRs fueled by toxic H$_2$O$_2$ fuel. Subsequently, nontoxic malic acid was demonstrated as an efficient propulsion fuel for the visible-light-driven Cu$_2$O@carbon dot micromotor (Figure 12b).[155]

In addition, our group proposed another potential solution to reduce fuel toxicity, through utilizing reversible redox. Because the reversible redox couple is not consumed in the reaction, a much-reduced chemical concentration can be used, which improved biocompatibility (Figure 12c).[47,56,156] For any electrophoretic MNR, the swimming speed (U) is proportional to the current density (J) and reversely proportional to the diffusion coefficient of charged ion (D_{ion}) as $U \propto \frac{J}{D_{ion}}$.[157–159] Based on this equation, we identified a group of reversible redox-active but diffusion-sluggish redox couples with outstanding propulsion efficiency at biocompatible dosage, as shown in Figure 12c.[156] To clearly compare different supporting chemical's toxicity–efficiency performance, the cell viability of chemicals should be tested and plotted against the relative propulsion efficiency with a series of supporting chemical concentrations. As shown in Figure 12d, Ferrocenemethanol (MFc) showed a better balance between the propulsion efficiency and relative viability in comparison with traditional chemicals. However, it is worth noting that the MFc is merely a demo redox couple, which is not yet suitable for practical application. Other redox-active and biocompatible couple is still needed for biomedical application.

We summarized the efficiencies of a series of representative LMNRs for comparison, as shown in **Table 1**. In general, the efficiencies of self-electrophoretic catalytic motors are around the order of 10^{-9},[158] whereas the efficiencies of thermophoresis and opto-thermoelectric LMNRs are even lower. With the progress of this area toward application, the efficiency should be improved significantly, which requires both improved fundamental understanding as well as technological breakthroughs.[160]

5.4. Alleviation of the Biofouling

As discussed earlier, controlled motion and transport of cargos at the micro/nanoscale by remote steering of MNRs is a promising technique for complex tasks, such as targeted drug delivery,[161–163] active detection,[164,165] and deep tumor penetration.[4,132,140] However, when deployed in a biological fluid, biofouling due to the passive immune response or nonspecific adsorption of proteins will detrimentally affect the performance of MNRs.[166,167] Hence, MNRs engineering for improved immunosuppression, long circulation, and anti-biofouling must be considered for the real application in biological environments.

To realize biofouling resistance, cell membrane-camouflage was applied as an excellent strategy.[140,166,168,169] For instance, the red blood cell membrane was demonstrated to camouflage the ultrasound-propelled nanomotor, serving as a motile sponge for efficient toxin decoying. Similarly, Wu et al. developed a macrophage cell membrane cloaked NIR-powered Janus mesoporous silica nanomotor, which can actively seek cancer cells and
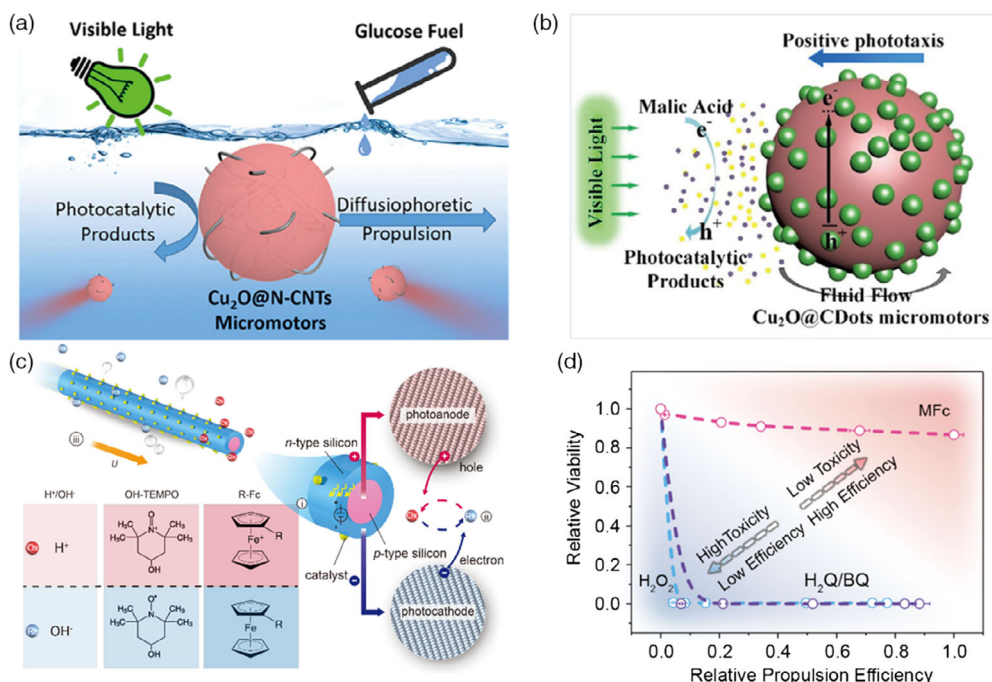
2000170 (13 of 18)

**ADVANCED
SCIENCE NEWS**

www.advancedsciencenews.com

**ADVANCED
INTELLIGENT
SYSTEMS**
Open Access

www.advintellsyst.com

Figure 12. Biocompatible and high-efficiency fuels for LMNR propulsion. a) Highly-efficient glucose-fueled Cu_2O@N-CNT micromotor. Reproduced with permission.[154] Copyright 2019, American Chemical Society. b) Malic acid as the biocompatible fuel for the propulsion of light-driven Cu_2O@carbon dot micromotor. Reproduced with permission.[155] Copyright 2020, Wiley-VCH. c) Schematic of the light-driven microswimmer that converts incident photon into mechanical propulsion with the aid of reversible redox shuttles. Reproduced with permission.[156] Copyright 2019, American Chemical Society. d) Phase diagram for the relative propulsion efficiency and toxicity (relative viability of cell) of different chemicals MFc, red dots; H_2Q/BQ, purple dots; H_2O_2, blue dots). Reproduced with permission.[156] Copyright 2019, American Chemical Society.

Table 1. Representative LMNRs and their material, size, mechanism, fuel, light intensity, speed, and efficiency.

Materials	Size [μm]	Mechanism	Supporting chemicals	Light intensity	Speed [μm s^{-1}]	Efficiency
Cu_2O@CDot sphere[155]	1.5 (D)	Self-electrophoresis	25 μM malic acid	≈150 mW cm^{-2} green light	40.85	7.5×10^{-9} a)
Pt/TiO_2 Janus sphere[176]	2.2 (D)	Self-electrophoresis	Pure water	40 mW cm^{-2} UV	8.9	9.6×10^{-10}
TiO_2–Au/Ag Janus sphere[177]	2 (D)	Self-electrophoresis	0.5 wt% H_2O_2	600 mW cm^{-2} UV	≈15	2×10^{-10} a)
p–n silicon nanowire[156]	0.5 (D)	Self-electrophoresis	70 μM ferrocenemethanol	≈70 mW cm^{-2} visible-light	≈500	2.3×10^{-6}
	≈10 (L)					
Cu_2O@N-CNT sphere[154]	1.5 (D)	Self-electrophoresis	30 mM glucose	≈150 mW cm^{-2} green light	18.7	1.6×10^{-9} a)
Sb_2Se_3/ZnO nanowire[56]	1 (D)	Self-electrophoresis	(10 mM/20 mM) BQ/H_2Q	≈600 mW cm^{-2} visible-light	≈15	4.3×10^{-11}
	≈20 (L)					
BiOI/metal Janus sphere[63]	2 (D)	Self-electrophoresis	Pure water	≈220 mW cm^{-2} green light	≈1.62	1.1×10^{-11}
CdS/C_{60} tube[178]	5 (D)	Bubble propulsion	5 wt% H_2O_2	UV-green	1058 ± 72	3.6×10^{-6} a)
	10 (L)					
TiO_2 tubular microengine[179]	6 (D)	Bubble propulsion	15 wt% H_2O_2	1 mW cm^{-2} UV	264	1.4×10^{-8} a)
	≈90 (L)					
Twin-jet-engine-microsystem[68]	≈800 (L)	Bubble propulsion	10% H_2O_2	Radiowave	1100	–
Cu/SiO_2 Janus particles[69]	6 (D)	Bubble propulsion	Water/glycerol	X-ray	1	8.7×10^{-13} a)
Carbonaceous nanobottle[180]	0.5 (D)	Thermophoresis	Not needed	0.74 W cm^{-2}	≈21	1.3×10^{-9}
(PSS/PAH)$_{20}$Au rocket[181]	5 (D)	Thermophoresis	Not needed	2×10^6 W cm^{-2} NIR	160	3.7×10^{-15}
	50 (L)					
PS/Au Janus sphere[182]	2 (D)	Opto-thermoelectric	0.2 mM CTAC	4×10^3 W cm^{-2}	15	3.4×10^{-14}

a)The presented efficiencies are estimated from the mechanical energy and incident light energy, without considering the energy from consumed chemicals. The mechanical energy calculation is adapted from previously reported method.[158] D: diameter; L: length.

**ADVANCED
SCIENCE NEWS**

www.advancedsciencenews.com

**ADVANCED
INTELLIGENT
SYSTEMS**
Open Access

www.advintellsyst.com

thermomechanically percolate cell membranes. When exposed to the biological medium, the cell membrane can effectively prevent the adhering of biological blocks. Very recently, perfluorocarbon-coated "slippery" micropropellers was prepared, which can readily pass through the vitreous humor to reach the retina.[170]

For chemical reaction powered MNRs, the chemical diffusion rate through the anti-biofouling coating must be considered. Fortunately, the antifouling coating has been intensively developed in the area of electrochemical (bio)sensing, which should also consider the trade-off between biofouling and diffusion limitation. To prevent fouling in electrochemical biosensing, nanoporous electrodes, carbon materials, and (bio)materials modification were proposed. Particularly, surface modifications, ranging from polymers, hydrogels, peptides, to thiolated self-assembled monolayers, have been well demonstrated.[171–174] Our group tested the sulfonated polystyrene (SPS)-coated microswimmer in the human blood medium and found the enhanced antifouling effect,[142] while better coating layers should be developed in the future for better biocompatibility.

6. Outlook and Conclusion

In this review, we first summarized the primary encoding modes of LMNRs. Frequency, spatial encoding, and polarization are three major metrics of light, and the encoding of them offers unusual control over LMNRs, at both individual and ensemble level. Such encoding modes also grant LMNRs sophisticated functions, which can bring about unprecedented applications with the help of the state-of-the-art onboard electronics. On top of that, considerable progress has been made for the design of LMNRs with hybridized magnetic, acoustic, or electric-field encoding, which further broadened the horizon of LMNRs design.

On the other hand, collective behaviors of LMNRs, including swarming and assembly, are quite tempting for their analogy with social animals and the potential to perform complex tasks. With the continuous discovery of new swarming phenomena and the investigation on the underlying mechanisms, a variety of applications can be expected.

Although many concepts have been proved for LMNRs, several critical bottlenecks still need to be addressed before the real applications can be achieved in biological environments. The toxicity of fuels, the presence of high concentration electrolytes, and the proteins in biological fluids, are still calling for the breakthrough in LMNRs. Recently, a novel light-driven microrobot was demonstrated with onboard circuitry,[175] which can operate by electrochemically induced stresses within a large range of environmental pH conditions. This electronically integrated robot may allow autonomous interaction with the surrounding biological environment using local sensory input and feedback, paving the way to a truly intelligent system driven by light.

Conflict of Interest

The authors declare no conflict of interest.

[1] L. Xu, F. Mou, H. Gong, M. Luo, J. Guan, *Chem. Soc. Rev.* **2017**, *46*, 6905.

[2] K. Villa, M. Pumera, *Chem. Soc. Rev.* **2019**, *48*, 4966.

[3] H. Šípová-Jungová, D. Andrén, S. Jones, M. Käll, *Chem. Rev.* **2020**, *120*, 269.

[4] W. Wang, Z. Wu, X. Lin, T. Si, Q. He, *J. Am. Chem. Soc.* **2019**, *141*, 6601.

[5] J. Wang, Z. Xiong, J. Zheng, X. Zhan, J. Tang, *Acc. Chem. Res.* **2018**, *51*, 1957.

[6] J. Li, W. Gao, R. Dong, A. Pei, S. Sattayasamitsathit, J. Wang, *Nat. Commun.* **2014**, *5*, 5026.

[7] Y. Wang, C. Zhou, W. Wang, D. Xu, F. Zeng, C. Zhan, J. Gu, M. Li, W. Zhao, J. Zhang, J. Guo, H. Feng, X. Ma, *Angew. Chem. Int. Ed.* **2018**, *57*, 13110.

[8] M. Safdar, S. U. Khan, J. Jänis, *Adv. Mater.* **2018**, 1703660.

[9] Z. Wu, L. Li, Y. Yang, P. Hu, Y. Li, S.-Y. Yang, L. V. Wang, W. Gao, *Sci. Robot.* **2019**, *4*, eaax0613.

[10] X. Yan, Q. Zhou, M. Vincent, Y. Deng, J. Yu, J. Xu, T. Xu, T. Tang, L. Bian, Y.-X. J. Wang, K. Kostarelos, L. Zhang, *Sci. Robot.* **2017**, *2*, eaaq1155.

[11] J. Li, B. Esteban-Fernández de Ávila, W. Gao, L. Zhang, J. Wang, *Sci. Robot.* **2017**, *2*, eaam6431.

[12] Y. Huang, Z. Liang, M. Alsoraya, J. Guo, D. Fan, *Adv. Intell. Syst.* **2020**, *2*, 1900127.

[13] X.-Z. Chen, M. Hoop, F. Mushtaq, E. Siringil, C. Hu, B. J. Nelson, S. Pané, *Appl. Mater. Today* **2017**, *9*, 37.

[14] L. Ren, W. Wang, T. E. Mallouk, *Acc. Chem. Res.* **2018**, *51*, 1948.

[15] K. K. Dey, A. Sen, *J. Am. Chem. Soc.* **2017**, *139*, 7666.

[16] T. Patiño, X. Arqué, R. Mestre, L. Palacios, S. Sánchez, *Acc. Chem. Res.* **2018**, *51*, 2662.

[17] M. Sitti, D. S. Wiersma, *Adv. Mater.* **2020**, *32*, 1906766.

[18] D. Fan, Z. Yin, R. Cheong, F. Q. Zhu, R. C. Cammarata, C. L. Chien, A. Levchenko, *Nat. Nanotechnol.* **2010**, *5*, 545.

[19] W. F. Paxton, P. T. Baker, T. R. Kline, Y. Wang, T. E. Mallouk, A. Sen, *J. Am. Chem. Soc.* **2006**, *128*, 14881.

[20] J. Wang, Z. Xiong, X. Zhan, B. Dai, J. Zheng, J. Liu, J. Tang, *Adv. Mater.* **2017**, *29*, 1701451.

[21] W. Duan, R. Liu, A. Sen, *J. Am. Chem. Soc.* **2013**, *135*, 1280.

[22] H.-R. Jiang, N. Yoshinaga, M. Sano, *Phys. Rev. Lett.* **2010**, *105*, 268302.

[23] M. Xuan, Z. Wu, J. Shao, L. Dai, T. Si, Q. He, *J. Am. Chem. Soc.* **2016**, *138*, 6492.

**ADVANCED
SCIENCE NEWS**

www.advancedsciencenews.com

**ADVANCED
INTELLIGENT
SYSTEMS**
Open Access

www.advintellsyst.com

[24] E. Karshalev, B. Esteban-Fernández de Ávila, J. Wang, *J. Am. Chem. Soc.* **2018**, *140*, 3810.

[25] H. Zeng, P. Wasylczyk, C. Parmeggiani, D. Martella, M. Burresi, D. S. Wiersma, *Adv. Mater.* **2015**, *27*, 3883.

[26] S. Palagi, A. G. Mark, S. Y. Reigh, K. Melde, T. Qiu, H. Zeng, C. Parmeggiani, D. Martella, A. Sanchez-Castillo, N. Kapernaum, *Nat. Mater.* **2016**, *15*, 647.

[27] A. Haeger, K. Wolf, M. M. Zegers, P. Friedl, *Trends Cell Biol.* **2015**, *25*, 556.

[28] D. T. Tambe, C. Corey Hardin, T. E. Angelini, K. Rajendran, C. Y. Park, X. Serra-Picamal, E. H. Zhou, M. H. Zaman, J. P. Butler, D. A. Weitz, J. J. Fredberg, X. Trepat, *Nat. Mater.* **2011**, *10*, 469.

[29] P. Friedl, D. Gilmour, *Nat. Rev. Mol. Cell Biol.* **2009**, *10*, 445.

[30] S. Li, R. Batra, D. Brown, H.-D. Chang, N. Ranganathan, C. Hoberman, D. Rus, H. Lipson, *Nature* **2019**, *567*, 361.

[31] M. Rubenstein, A. Cornejo, R. Nagpal, *Science* **2014**, *345*, 795.

[32] H. Chen, Q. Zhao, X. Du, *Micromachines* **2018**, *9*, 41.

[33] H. Wang, M. Pumera, *Chem. Rev.* **2015**, *115*, 8704.

[34] A. Ashkin, J. M. Dziedzic, J. E. Bjorkholm, S. Chu, *Opt. Lett.* **1986**, *11*, 288.

[35] T. Wu, T. A. Nieminen, S. Mohanty, J. Miotke, R. L. Meyer, H. Rubinsztein-Dunlop, M. W. Berns, *Nat. Photon.* **2012**, *6*, 62.

[36] L. Bosanac, T. Aabo, P. M. Bendix, L. B. Oddershede, *Nano. Lett.* **2008**, *8*, 1486.

[37] P. M. Hansen, V. K. Bhatia, N. Harrit, L. Oddershede, *Nano. Lett.* **2005**, *5*, 1937.

[38] U. G. Būtaitė, G. M. Gibson, Y.-L. D. Ho, M. Taverne, J. M. Taylor, D. B. Phillips, *Nat. Commun.* **2019**, *10*, 1215.

[39] D. B. Phillips, M. J. Padgett, S. Hanna, Y. L. D. Ho, D. M. Carberry, M. J. Miles, S. H. Simpson, *Nat. Photon.* **2014**, *8*, 400.

[40] S. Kawata, H.-B. Sun, T. Tanaka, K. Takada, *Nature* **2001**, *412*, 697.

[41] E. J. G. Peterman, F. Gittes, C. F. Schmidt, *Biophys. J.* **2003**, *84*, 1308.

[42] P. Y. Chiou, A. T. Ohta, M. C. Wu, *Nature* **2005**, *436*, 370.

[43] S. Zhang, E. Y. Scott, J. Singh, Y. Chen, Y. Zhang, M. Elsayed, M. D. Chamberlain, N. Shakiba, K. Adams, S. Yu, C. M. Morshead, P. W. Zandstra, A. R. Wheeler, *Proc. Natl. Acad. Sci.* **2019**, *116*, 14823.

[44] J. Wang, J.-Y. Yang, I. M. Fazal, N. Ahmed, Y. Yan, H. Huang, Y. Ren, Y. Yue, S. Dolinar, M. Tur, A. E. Willner, *Nat. Photon.* **2012**, *6*, 488.

[45] G. Knöner, S. Parkin, T. A. Nieminen, V. L. Y. Loke, N. R. Heckenberg, H. Rubinsztein-Dunlop, *Opt. Express* **2007**, *15*, 5521.

[46] K.-I. Wakabayashi, Y. Misawa, S. Mochiji, R. Kamiya, *Proc. Natl. Acad. Sci.* **2011**, *108*, 11280.

[47] B. Dai, J. Wang, Z. Xiong, X. Zhan, W. Dai, C.-C. Li, S.-P. Feng, J. Tang, *Nat. Nanotechnol.* **2016**, *11*, 1087.

[48] C. Chen, F. Mou, L. Xu, S. Wang, J. Guan, Z. Feng, Q. Wang, L. Kong, W. Li, J. Wang, Q. Zhang, *Adv. Mater.* **2017**, *29*, 1603374.

[49] Z. Ye, Y. Sun, H. Zhang, B. Song, B. Dong, *Nanoscale* **2017**, *9*, 18516.

[50] L. Kong, C. C. Mayorga-Martinez, J. Guan, M. Pumera, *Chem. Asian J.* **2019**, *14*, 2456.

[51] D. Zhang, Y. Sun, M. Li, H. Zhang, B. Song, B. Dong, *J. Mater. Chem. C* **2018**, *6*, 12234.

[52] L. Tong, V. D. Miljković, M. Käll, *Nano. Lett.* **2010**, *10*, 268.

[53] L. Shao, M. Käll, *Adv. Funct. Mater.* **2018**, *28*, 1706272.

[54] A. Lehmuskero, R. Ogier, T. Gschneidtner, P. Johansson, M. Käll, *Nano. Lett.* **2013**, *13*, 3129.

[55] L. Shao, Z.-J. Yang, D. Andrén, P. Johansson, M. Käll, *ACS Nano* **2015**, *9*, 12542.

[56] X. Zhan, J. Zheng, Y. Zhao, B. Zhu, R. Cheng, J. Wang, J. Liu, J. Tang, J. Tang, *Adv. Mater.* **2019**, *31*, 1903329.

[57] M. Wolffs, S. J. George, Ž. Tomović, S. C. J. Meskers, A. P. H. J. Schenning, E. W. Meijer, *Angew. Chem. Int. Ed.* **2007**, *46*, 8203.

[58] C. Song, M. G. Blaber, G. Zhao, P. Zhang, H. C. Fry, G. C. Schatz, N. L. Rosi, *Nano. Lett.* **2013**, *13*, 3256.

[59] F. Han, J. A. Parker, Y. Yifat, C. Peterson, S. K. Gray, N. F. Scherer, Z. Yan, *Nat. Commun.* **2018**, *9*, 4897.

[60] E. Yashima, N. Ousaka, D. Taura, K. Shimomura, T. Ikai, K. Maeda, *Chem. Rev.* **2016**, *116*, 13752.

[61] L. Cong, N. Xu, J. Gu, R. Singh, J. Han, W. Zhang, *Laser Photonics Rev.* **2014**, *8*, 626.

[62] B. Jang, A. Hong, H. E. Kang, C. Alcantara, S. Charreyron, F. Mushtaq, E. Pellicer, R. Büchel, J. Sort, S. S. Lee, B. J. Nelson, S. Pané, *ACS Nano* **2017**, *11*, 6146.

[63] R. Dong, Y. Hu, Y. Wu, W. Gao, B. Ren, Q. Wang, Y. Cai, *J. Am. Chem. Soc.* **2017**, *139*, 1722.

[64] C. Maggi, F. Saglimbeni, M. Dipalo, F. De Angelis, R. Di Leonardo, *Nat. Commun.* **2015**, *6*, 7855.

[65] M. Wan, Q. Wang, R. Wang, R. Wu, T. Li, D. Fang, Y. Huang, Y. Yu, L. Fang, X. Wang, Y. Zhang, Z. Miao, B. Zhao, F. Wang, C. Mao, Q. Jiang, X. Xu, D. Shi, *Sci. Adv.* **2020**, *6*, eaaz9014.

[66] M. Wan, Q. Wang, X. Li, B. Xu, D. Fang, T. Li, Y. Yu, L. Fang, Y. Wang, M. Wang, F. Wang, C. Mao, J. Shen, J. Wei, *Angew. Chem. Int. Ed.* **2020**, *59*, 14458.

[67] X. Zhou, Z. Li, L. Tan, Y. Zhang, Y. Jiao, *ACS Appl. Mater. Inter.* **2020**, *12*, 23134.

[68] V. K. Bandari, Y. Nan, D. Karnaushenko, Y. Hong, B. Sun, F. Striggow, D. D. Karnaushenko, C. Becker, M. Faghih, M. Medina-Sánchez, F. Zhu, O. G. Schmidt, *Nat. Electron.* **2020**, *3*, 172.

[69] Z. Xu, M. Chen, H. Lee, S.-P. Feng, J. Y. Park, S. Lee, J. T. Kim, *ACS Appl. Mater. Inter.* **2019**, *11*, 15727.

[70] O. Ilic, I. Kaminer, Y. Lahini, H. Buljan, M. Soljačić, *ACS Photonics* **2016**, *3*, 197.

[71] É. O'Neel-Judy, D. Nicholls, J. Castañeda, J. G. Gibbs, *Small* **2018**, *14*, 1801860.

[72] J. Zheng, J. Wang, Z. Xiong, Z. Wan, X. Zhan, S. Yang, J. Chen, J. Dai, J. Tang, *Adv. Funct. Mater.* **2019**, *29*, 1901768.

[73] J. Zheng, B. Dai, J. Wang, Z. Xiong, Y. Yang, J. Liu, X. Zhan, Z. Wan, J. Tang, *Nat. Commun.* **2017**, *8*, 1438.

[74] J. Palacci, S. Sacanna, A. Vatchinsky, P. M. Chaikin, D. J. Pine, *J. Am. Chem. Soc.* **2013**, *135*, 15978.

[75] D. Zhou, L. Ren, Y. C. Li, P. Xu, Y. Gao, G. Zhang, W. Wang, T. E. Mallouk, L. Li, *Chem. Commun.* **2017**, *53*, 11465.

[76] C. Wang, R. Dong, Q. Wang, C. Zhang, X. She, J. Wang, Y. Cai, *Chem. Asian J.* **2019**, *14*, 2485.

[77] Q. Wang, C. Wang, R. Dong, Q. Pang, Y. Cai, *Inorg. Chem. Commun.* **2018**, *91*, 1.

[78] V. Sridhar, B.-W. Park, M. Sitti, *Adv. Funct. Mater.* **2018**, *28*, 1704902.

[79] D. Wang, G. Zhao, C. Chen, H. Zhang, R. Duan, D. Zhang, M. Li, B. Dong, *Langmuir* **2019**, *35*, 2801.

[80] D. Zhou, Y. Gao, J. Yang, Y. C. Li, G. Shao, G. Zhang, T. Li, L. Li, *Adv. Sci.* **2018**, *5*, 1800122.

[81] Z. Liang, D. Teal, D. Fan, *Nat. Commun.* **2019**, *10*, 5275.

[82] Z. Liang, D. Fan, *Sci. Adv.* **2018**, *4*, eaau0981.

[83] J. K. Parrish, L. Edelstein-Keshet, *Science* **1999**, *284*, 99.

[84] M. C. Marchetti, J.-F. Joanny, S. Ramaswamy, T. B. Liverpool, J. Prost, M. Rao, R. A. Simha, *Rev. Mod. Phys.* **2013**, *85*, 1143.

[85] G. M. Whitesides, B. Grzybowski, *Science* **2002**, *295*, 2418.

[86] T. Xu, L.-P. Xu, X. Zhang, *Appl. Mater. Today* **2017**, *9*, 493.

[87] X. Ma, A. C. Hortelão, T. Patiño, S. Sánchez, *ACS Nano* **2016**, *10*, 9111.

[88] W. Wang, W. Duan, S. Ahmed, A. Sen, T. E. Mallouk, *Acc. Chem. Res.* **2015**, *48*, 1938.

[89] J. Zhang, J. Guo, F. Mou, J. Guan, *Micromachines* **2018**, *9*, 88.

[90] M. You, C. Chen, L. Xu, F. Mou, J. Guan, *Acc. Chem. Res.* **2018**, *51*, 3006.

2000170 (16 of 18)

[91] A. A. Solovev, S. Sanchez, O. G. Schmidt, *Nanoscale* **2013**, *5*, 1284.

[92] H. Wang, M. Pumera, *Chem. Soc. Rev.* **2020**, *49*, 3211.

[93] V. Yadav, H. Zhang, R. Pavlick, A. Sen, *J. Am. Chem. Soc.* **2012**, *134*, 15688.

[94] M. Ibele, T. E. Mallouk, A. Sen, *Angew. Chem. Int. Ed.* **2009**, *48*, 3308.

[95] Y. Hong, M. Diaz, U. M. Córdova-Figueroa, A. Sen, *Adv. Funct. Mater.* **2010**, *20*, 1568.

[96] X. Chen, C. Zhou, Y. Peng, Q. Wang, W. Wang, *ACS Appl. Mater. Interfaces* **2020**, *12*, 11843.

[97] C. Zhou, X. Chen, Z. Han, W. Wang, *ACS Nano* **2019**, *13*, 4064.

[98] C. Zhou, N. J. Suematsu, Y. Peng, Q. Wang, X. Chen, Y. Gao, W. Wang, *ACS Nano* **2020**, *14*, 5360.

[99] C. Zhou, Q. Wang, X. Lv, W. Wang, *Chem. Commun.* **2020**, *56*, 6499.

[100] J. Palacci, S. Sacanna, A. P. Steinberg, D. J. Pine, P. M. Chaikin, *Science* **2013**, *339*, 936.

[101] A. Aubret, M. Youssef, S. Sacanna, J. Palacci, *Nat. Phys.* **2018**, *14*, 1114.

[102] D. P. Singh, U. Choudhury, P. Fischer, A. G. Mark, *Adv. Mater.* **2017**, *29*, 1701328.

[103] F. Mou, L. Kong, C. Chen, Z. Chen, L. Xu, J. Guan, *Nanoscale* **2016**, *8*, 4976.

[104] Y. Gao, F. Mou, S. Che, W. Li, L. Xu, J. Guan, *ACS Appl. Mater. Interfaces* **2017**, *9*, 22704.

[105] X. Liang, F. Mou, Z. Huang, J. Zhang, M. You, L. Xu, M. Luo, J. Guan, *Adv. Funct. Mater.* **2020**, *30*, 1908602.

[106] Q. Zhang, R. Dong, X. Chang, B. Ren, Z. Tong, *ACS Appl. Mater. Interfaces* **2015**, *7*, 24585.

[107] D. G. Grier, *Nature* **2003**, *424*, 810.

[108] J. R. Moffitt, Y. R. Chemla, S. B. Smith, C. Bustamante, *Annu. Rev. Biochem.* **2008**, *77*, 205.

[109] A. Lehmuskero, P. Johansson, H. Rubinsztein-Dunlop, L. Tong, M. Käll, *ACS Nano* **2015**, *9*, 3453.

[110] K. Y. Chen, A. T. Lee, C. C. Hung, J. S. Huang, Y. T. Yang, *Nano. Lett.* **2013**, *13*, 4118.

[111] E. Jaquay, L. J. Martínez, C. A. Mejia, M. L. Povinelli, *Nano. Lett.* **2013**, *13*, 2290.

[112] F. M. Weinert, D. Braun, *Phys. Rev. Lett.* **2008**, *101*, 168301.

[113] R. Golestanian, *Phys. Rev. Lett.* **2012**, *108*, 038303.

[114] J. A. Cohen, R. Golestanian, *Phys. Rev. Lett.* **2014**, *112*, 068302.

[115] L. Lin, X. Peng, M. Wang, L. Scarabelli, Z. Mao, L. M. Liz-Marzán, M. F. Becker, Y. Zheng, *ACS Nano* **2016**, *10*, 9659.

[116] L. Lin, J. Zhang, X. Peng, Z. Wu, A. C. Coughlan, Z. Mao, M. A. Bevan, Y. Zheng, *Sci. Adv.* **2017**, *3*, e1700458.

[117] Z. Deng, F. Mou, S. Tang, L. Xu, M. Luo, J. Guan, *Appl. Mater. Today* **2018**, *13*, 45.

[118] D. Zhou, Y. Gao, H. Liu, G. Zhang, L. Li, *Chem. Asian J.* **2019**, *14*, 2445.

[119] Y. Sun, Y. Liu, D. Zhang, H. Zhang, J. Jiang, R. Duan, J. Xiao, J. Xing, D. Zhang, B. Dong, *ACS Appl. Mater. Inter.* **2019**, *11*, 40533.

[120] F. Mou, J. Zhang, Z. Wu, S. Du, Z. Zhang, L. Xu, J. Guan, *iScience* **2019**, *19*, 415.

[121] D. P. Singh, A. Domínguez, U. Choudhury, S. N. Kottapalli, M. N. Popescu, S. Dietrich, P. Fischer, *Nat. Commun.* **2020**, *11*, 2210.

[122] S. Johnson, *Emergence: The Connected Lives Of Ants, Brains, Cities, And Software*, Scribner, New York, NY **2002**.

[123] J. Li, V. V. Singh, S. Sattayasamitsathit, J. Orozco, K. Kaufmann, R. Dong, W. Gao, B. Jurado-Sanchez, Y. Fedorak, J. Wang, *ACS Nano* **2014**, *8*, 11118.

[124] D. Uygun, B. Jurado-Sánchez, M. Uygun, J. Wang, *Environ. Sci.: Nano* **2016**, *3*, 559.

[125] Y. Wu, R. Dong, Q. Zhang, B. Ren, *Nano-Micro Lett.* **2017**, *9*, 30.

[126] Q. Zhang, R. Dong, Y. Wu, W. Gao, Z. He, B. Ren, *ACS Appl. Mater. Interfaces* **2017**, *9*, 4674.

[127] K. Villa, C. L. Manzanares Palenzuela, Z. k. Sofer, S. Matějková, M. Pumera, *ACS Nano* **2018**, *12*, 12482.

[128] K. Villa, F. Novotný, J. Zelenka, M. P. Browne, T. S. Ruml, M. Pumera, *ACS Nano* **2019**, *13*, 8135.

[129] M. Enachi, M. Guix, V. Postolache, V. Ciobanu, V. M. Fomin, O. G. Schmidt, I. J. Tiginyanu, *Small* **2016**, *12*, 5497.

[130] M. Paven, H. Mayama, T. Sekido, H. J. Butt, Y. Nakamura, S. Fujii, *Adv. Funct. Mater.* **2016**, *26*, 3199.

[131] Z. Wu, X. Lin, Y. Wu, T. Si, J. Sun, Q. He, *ACS Nano* **2014**, *8*, 6097.

[132] X. Jiao, Z. Wang, J. Xiu, W. Dai, L. Zhao, T. Xu, X. Du, Y. Wen, X. Zhang, *Appl. Mater. Today* **2020**, *18*, 100504.

[133] W. Liu, W. Wang, X. Dong, Y. Sun, *ACS Appl. Mater. Interfaces* **2020**, *12*, 12618.

[134] S. Wang, X. Liu, Y. Wang, D. Xu, C. Liang, J. Guo, X. Ma, *Nanoscale* **2019**, *11*, 14099.

[135] J. Ou, K. Liu, J. Jiang, D. A. Wilson, L. Liu, F. Wang, S. Wang, Y. Tu, F. Peng, *Small* **2020**, *16*, 1906184.

[136] D. Wang, C. Gao, W. Wang, M. Sun, B. Guo, H. Xie, Q. He, *ACS Nano* **2018**, *12*, 10212.

[137] H. Choi, G.-H. Lee, K. S. Kim, S. K. Hahn, *ACS Appl. Mater. Interfaces* **2018**, *10*, 2338.

[138] C. Gao, Z. Lin, D. Wang, Z. Wu, H. Xie, Q. He, *ACS Appl. Mater. Inter.* **2019**, *11*, 23392.

[139] D. Xu, C. Zhou, C. Zhan, Y. Wang, Y. You, X. Pan, J. Jiao, R. Zhang, Z. Dong, W. Wang, X. Ma, *Adv. Funct. Mater.* **2019**, *29*, 1807727.

[140] M. Xuan, J. Shao, C. Gao, W. Wang, L. Dai, Q. He, *Angew. Chem. Int. Ed.* **2018**, *57*, 12463.

[141] S. Du, H. Wang, C. Zhou, W. Wang, Z. Zhang, *J. Am. Chem. Soc.* **2020**, *142*, 2213.

[142] X. Zhan, J. Wang, Z. Xiong, X. Zhang, Y. Zhou, J. Zheng, J. Chen, S.-P. Feng, J. Tang, *Nat. Commun.* **2019**, *10*, 3921.

[143] K. K. Dey, S. Das, M. F. Poyton, S. Sengupta, P. J. Butler, P. S. Cremer, A. Sen, *ACS Nano* **2014**, *8*, 11941.

[144] K. K. Dey, X. Zhao, B. M. Tansi, W. J. Méndez-Ortiz, U. M. Córdova-Figueroa, R. Golestanian, A. Sen, *Nano Lett.* **2015**, *15*, 8311.

[145] F. Mou, C. Chen, Q. Zhong, Y. Yin, H. Ma, J. Guan, *ACS Appl. Mater. Interfaces* **2014**, *6*, 9897.

[146] A. C. Hortelão, T. Patiño, A. Perez-Jiménez, À. Blanco, S. Sánchez, *Adv. Funct. Mater.* **2018**, *28*, 1705086.

[147] D. A. Wilson, R. J. Nolte, J. C. Van Hest, *Nat. Chem.* **2012**, *4*, 268.

[148] M. Pacheco, B. Jurado-Sánchez, A. Escarpa, *Angew. Chem. Int. Ed.* **2019**, *58*, 18017.

[149] R. Liu, A. Sen, *J. Am. Chem. Soc.* **2011**, *133*, 20064.

[150] W. F. Paxton, K. C. Kistler, C. C. Olmeda, A. Sen, S. K. St. Angelo, Y. Cao, T. E. Mallouk, P. E. Lammert, V. H. Crespi, *J. Am. Chem. Soc.* **2004**, *126*, 13424.

[151] M. E. Ibele, Y. Wang, T. R. Kline, T. E. Mallouk, A. Sen, *J. Am. Chem. Soc.* **2007**, *129*, 7762.

[152] W. Gao, A. Pei, R. Dong, J. Wang, *J. Am. Chem. Soc.* **2014**, *136*, 2276.

[153] F. Wong, A. Sen, *ACS Nano* **2016**, *10*, 7172.

[154] Q. Wang, R. Dong, C. Wang, S. Xu, D. Chen, Y. Liang, B. Ren, W. Gao, Y. Cai, *ACS Appl. Mater. Interfaces* **2019**, *11*, 6201.

[155] J. Wang, H. Wu, X. Liu, Q. Liang, Z. Bi, Z. Wang, Y. Cai, R. Dong, *Adv. Intell. Syst.* **2020**, *2*, 1900159.

[156] J. Wang, Z. Xiong, M. Liu, X. M. Li, J. Zheng, X. Zhan, W. Ding, J. Chen, X. Li, X. D. Li, S. P. Feng, J. Tang, *ACS Nano* **2020**, *14*, 3272.

[157] J. L. Moran, J. D. Posner, *Phys. Fluids* **2014**, *26*, 042001.

[158] W. Wang, T.-Y. Chiang, D. Velegol, T. E. Mallouk, *J. Am. Chem. Soc.* **2013**, *135*, 10557.

[159] A. T. Brown, W. C. Poon, C. Holm, J. J. S. M. de Graaf, *Soft Matter* **2017**, *13*, 1200.

[160] D. Zhou, R. Zhuang, X. Chang, L. Li, *Research* **2020**, *2020*, 6821595.

[161] Z. Wu, X. Lin, X. Zou, J. Sun, Q. He, *ACS Appl. Mater. Interfaces* **2015**, *7*, 250.

[162] X. Wang, X. Z. Chen, C. C. Alcântara, S. Sevim, M. Hoop, A. Terzopoulou, C. de Marco, C. Hu, A. J. de Mello, P. Falcaro, *Adv. Mater.* **2019**, *31*, 1901592.

[163] J. Shao, M. Xuan, Q. He, L. Dai, *Curr. Drug Targets* **2018**, *19*, 328.

[164] B. Esteban-Fernández de ávila, A. Martín, F. Soto, M. A. Lopez-Ramirez, S. Campuzano, G. M. Vasquez-Machado, W. Gao, L. Zhang, J. Wang, *ACS Nano* **2015**, *9*, 6756.

[165] A. Chałupniak, E. Morales-Narváez, A. Merkoçi, *Adv. Drug Deliv. Rev.* **2015**, *95*, 104.

[166] A. V. Kroll, R. H. Fang, L. Zhang, *Bioconjugate Chem.* **2017**, *28*, 23.

[167] C.-M. J. Hu, L. Zhang, S. Aryal, C. Cheung, R. H. Fang, L. Zhang, *Proc. Natl. Acad. Sci.* **2011**, *108*, 10980.

[168] Z. Wu, T. Li, W. Gao, T. Xu, B. Jurado-Sánchez, J. Li, W. Gao, Q. He, L. Zhang, J. Wang, *Adv. Funct. Mater.* **2015**, *25*, 3881.

[169] D. Wang, C. Gao, C. Zhou, Z. Lin, Q. He, *Research* **2020**, *2020*, 1.

[170] Z. Wu, J. Troll, H.-H. Jeong, Q. Wei, M. Stang, F. Ziemssen, Z. Wang, M. Dong, S. Schnichels, T. Qiu, P. Fischer, *Sci. Adv.* **2018**, *4*, eaat4388.

[171] S. Campuzano, M. Pedrero, P. Yáñez-Sedeño, J. M. Pingarrón, *Int. J. Mol. Sci.* **2019**, *20*, 423.

[172] I. Banerjee, R. C. Pangule, R. S. Kane, *Adv. Mater.* **2011**, *23*, 690.

[173] S. Chen, L. Li, C. Zhao, J. J. P. Zheng, *Polymer* **2010**, *51*, 5283.

[174] J. S. del Río, O. Y. Henry, P. Jolly, D. E. Ingber, *Nat. Nanotechnol.* **2019**, *14*, 1143.

[175] M. Z. Miskin, A. J. Cortese, K. Dorsey, E. P. Esposito, M. F. Reynolds, Q. Liu, M. Cao, D. A. Muller, P. L. McEuen, I. Cohen, *Nature* **2020**, *584*, 557.

[176] T. Maric, M. Z. M. Nasir, R. D. Webster, M. Pumera, *Adv. Funct. Mater.* **2020**, *30*, 1908614.

[177] Z. Xiao, J. Chen, S. Duan, X. Lv, J. Wang, X. Ma, J. Tang, W. Wang, *Chem. Commun.* **2020**, *56*, 4728.

[178] R. María Hormigos, B. Jurado Sánchez, A. Escarpa, *Angew. Chem. Int. Ed.* **2019**, *58*, 3128.

[179] F. Mou, Y. Li, C. Chen, W. Li, Y. Yin, H. Ma, J. Guan, *Small* **2015**, *11*, 2564.

[180] M. Xuan, R. Mestre, C. Gao, C. Zhou, Q. He, S. Sánchez, *Angew. Chem. Int. Ed.* **2018**, *57*, 6838.

[181] Z. Wu, T. Si, W. Gao, X. Lin, J. Wang, Q. He, *Small* **2016**, *12*, 577.

[182] X. Peng, Z. Chen, P. S. Kollipara, Y. Liu, J. Fang, L. Lin, Y. Zheng, *Light Sci. Appl.* **2020**, *9*, 141.

Jizhuang Wang is currently an associate professor in the College of Chemistry and Materials Science at Jinan University. He received Ph.D. degree in the Department of Chemistry at The University of Hong Kong under the supervision of Prof. Jinyao Tang in 2018. His current research interests are focusing on the micro/nanomotor design, mechanism study and related applications.
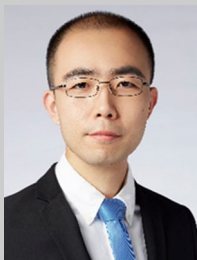
Ze Xiong received his Ph.D. in chemistry from The University of Hong Kong in 2017 and has been working as a research fellow at National University of Singapore since 2018. His research background combines materials science, chemistry, and engineering for the development of micro/nanorobots, biomedical electronics, and wearable sensors.

Jinyao Tang is an associate professor of the Chemistry Department at the University of Hong Kong. He received his Ph.D. from Columbia University in 2008 and was a postdoctoral researcher at UC Berkeley until 2012. Tang's group is focused on developing smart active colloidal particles, functional materials, and devices.